Inorganic Chemistry

Article

pubs.acs.org/IC

Anticancer Activity of Iridium(III) Complexes Based on a Pyrazole-Appended Quinoline-Based BODIPY

Rajendra Prasad Paitandi,[†] Sujay Mukhopadhyay,[†] Roop Shikha Singh,[†] Vinay Sharma,[‡] Shaikh M. Mobin,[‡,§,∥] and Daya Shankar Pandey*[,†]

[†]Department of Chemistry, Institute of Science, Banaras Hindu University, Varanasi 221005, Uttar Pradesh, India

[‡]Centre for Biosciences and Bio-Medical Engineering, [§]Discipline of Chemistry, and [∥]Metallurgical Engineering and Material Science, Indian Institute of Technology Indore, Simrol, Indore 453552, India

Supporting Information

ABSTRACT: A pyrazole-appended quinoline-based 4,4-difluoro-4-bora-3a,4a-diaza-*s*-indacene (**L1**, BODIPY) has been synthesized and used as a ligand for the preparation of iridium(III) complexes $[Ir(phpy)_2(\mathbf{L1})]PF_6$ (**1**; phpy = 2-phenylpyridine) and $[(\eta^5\text{-}C_5Me_5)Ir(\mathbf{L1})Cl]PF_6$ (**2**). The ligand **L1** and complexes **1** and **2** have been meticulously characterized by elemental analyses and spectral studies (IR, electrospray ionization mass spectrometry, ^1H and ^{13}C NMR, UV/vis, fluorescence) and their structures explicitly authenticated by single-crystal X-ray analyses. UV/vis, fluorescence, and circular dichroism studies showed that complexes strongly bind with calf-thymus DNA and bovine serum albumin. Molecular docking studies clearly illustrated binding through DNA minor grooves via van der Waals forces and their electrostatic interaction and occurrence in the hydrophobic cavity of protein (subdomain IIA). Cytotoxicity, morphological changes, and apoptosis have been explored by 3-(4,5-dimethylthiazol-2-yl)-2,5-diphenyltetrazolium bromide (MTT) assay and Hoechst 33342 staining. IC_{50} values for complexes (**1**, 30 μM; **2**, 50 μM) at 24 h toward the human cervical cancer cell line (HeLa) are as good as that of cisplatin (21.6 μM) under analogous conditions, and their ability to kill cancer cells lies in the order **1** > **2**. Because of the inherent emissive nature of the BODIPY moiety, these are apt for intracellular visualization at low concentration and may find potential applications in cellular imaging and behave as a theranostic agent.

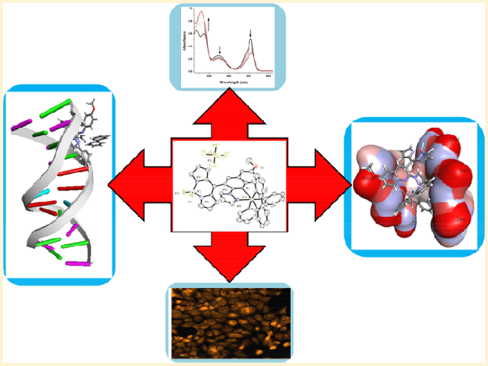

INTRODUCTION

The successful application of cisplatin and its derivatives in the treatment of a broad spectrum of cancers has stimulated the scientific community to develop other metal complexes exhibiting better anticancer activity.[1−6] Despite outstanding utility, the clinical value of platinum-based drugs is severely affected by serious side effects like high toxicity, drug selectivity, and intrinsic and acquired resistance.[7−9] To overcome these problems, metallodrugs containing organometallic moieties, metallocenes, and half-sandwich complexes have drawn special attention.[1,5,10−16] In this direction, the antiproliferative activity of some organometallic square-planar iridium(I) complexes, viz., [Ir(acac)(cod)], $[IrCl(cod)]_2$, etc., has been examined against various types of cancer.[17,18] Although these exhibit promising antiproliferative activity, their mechanism of action has not been established with certainty.[9] Considering this and the high stability of iridium(III) complexes, coupled with the significant structural diversity half-sandwich iridium(III) complexes, has been fascinating because some of these exhibited encouraging results. Additionally, it has been categorically shown that their action involves both an attack on DNA and a perturbation in the redox status of the cells.[19−22]

Furthermore, multifunctional theranostic agents have garnered significant clinical relevance because of their anticancer potencies besides their luminescent properties.[23−26] In this regard, cyclometalated iridium(III) complexes, because of their high quantum yield, large Stokes shift, long-lived luminescence, good photostability, and cell permeability, have attracted the attention of many research groups.[27−33,33] In addition, these enhance the electron density at the metal center and make it labile along with stabilizing high-valent metal complexes and augmenting the oxidizing ability via reactive oxygen species generation, causing cancer cell death.[35−37] The incorporation of an electron-rich pentamethylcyclopentadienyl moiety can have power over the balance between the hydrophobicity and hydrophilicity and enhance cellular uptake.[38] It is worth mentioning that cationic iridium(III) complexes can regulate covalent or noncovalent intercalation/interactions and augment anticancer activity because of their specific redox properties.[39−46] Thus, numerous half-sandwich cyclopentadienyliridium(III) complexes containing bidentate ligands (N^N, N^O, or C^N chelating) have been synthesized and shown to be extremely effective toward tumor cells.[11,47−50] Sadler et al. observed that replacement of the neutral N^N-donor 2,2′-bipyridine (bpy) by C^N-chelating 2-phenylpyridine

Received: July 3, 2017

DOI: 10.1021/acs.inorgchem.7b01693
Inorg. Chem. XXXX, XXX, XXX−XXX

Scheme 1. Syntheses of Ligand L1 and Complexes 1 and 2

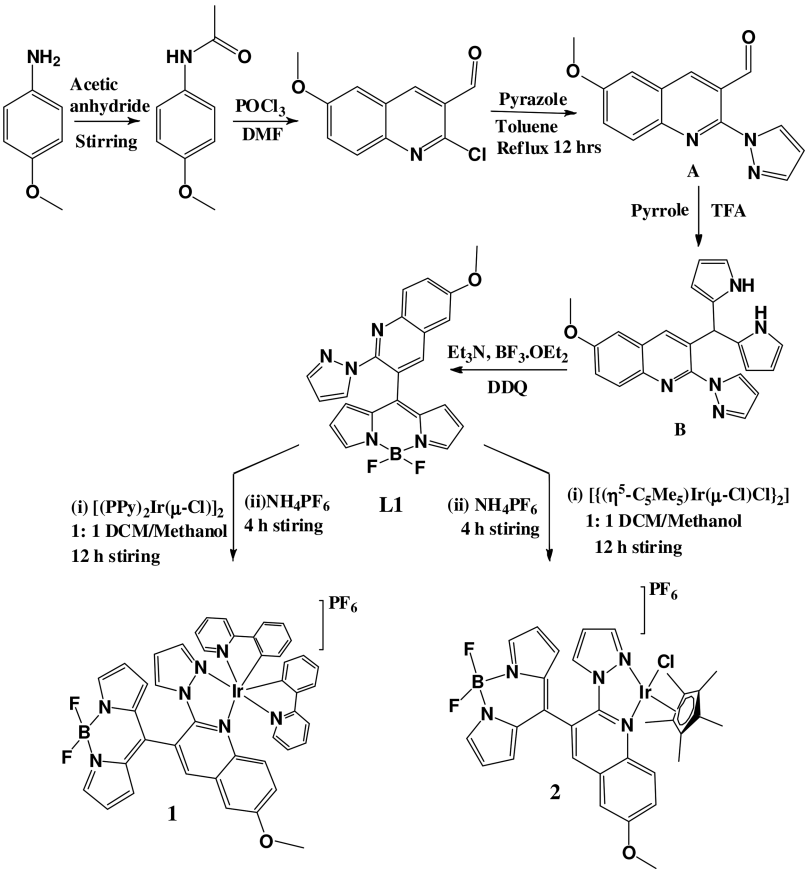

(phpy) in $[(\eta^5\text{-}C_5Me_5)Ir(bpy)Cl]^+$ improved its cytotoxic behavior against A2780 cells.[10,49] Also, they have thoroughly investigated the effect of changes of the negatively charged C^N-chelating ligand and the nature of diverse cyclopentadienyl groups on the biological properties.[11,48,50]

Additionally, intercalation of the drugs with a DNA helix inhibits enzyme replication.[51,52] Dipyrrin and its derivatives (4,4-difluoro-4-bora-3a,4a-diaza-*s*-indacene, BODIPY) are known to intercalate between base pairs of DNA and interfere with the transcription process, which can be exploited in the design of anticancer drugs.[53,54] Further, BODIPY dyes have been used as potential photodynamic therapeutic agents because of their ability to generate singlet oxygen.[55] Recently, Lee et al. developed some ruthenium(II), palladium(II), and iridium(III) metallarectangles containing a BODIPY-based linker and established that these exhibit highly selective anticancer activity, strongly interact with DNA and protein, and also display cellular localization.[41,56] We too have prepared some iridium(III) dipyrrinato complexes possessing diverse substituents like thioether, ferrocenyl, 2-methoxypyridyl, etc., and have shown that these interact with DNA and protein and exhibit prominent anticancer activity.[53,57,58] To develop efficient anticancer agents based on BODIPY-containing iridium(III) complexes through this work, we prepared a novel pyrazole-appended quinoline-based BODIPY (**L1**) and utilized it in the synthesis of cationic complexes $[Ir(phpy)_2(\mathbf{L1})]PF_6$ (**1**; phpy = 2-phenylpyridine) and $[(\eta^5\text{-}C_5Me_5)Ir(\mathbf{L1})Cl]PF_6$ (**2**). Through this contribution, we present the synthesis and thorough characterization of **L1** and cationic iridium(III) complexes **1** and **2**. Also, we describe herein their binding ability with DNA and protein and cytotoxicity against human cervical cancer cell line (HeLa) along with possible applications as a theranostic agent.

RESULTS AND DISCUSSION

Synthesis and Characterization. A methoxy derivative of 2-chloroquinoline-3-carbaldehyde has been synthesized by following literature procedures.[59] 6-Methoxy-2-(1*H*-pyrazol-1-yl)quinoline-3-carbaldehyde (**A**) was prepared by treating a solution of a quinoline aldehyde (2-chloroquinoline-3-carbaldehyde) in toluene with pyrazole under refluxing conditions and continual stirring (48 h). Aldehyde **A** reacted with an excess of pyrrole in the presence of trifluoroacetic acid to afford 5-[6-methoxy-2-(1*H*-pyrazol-1-yl)quinoline]dipyrromethane (**B**). The synthesis of **L1** was achieved from **B** via a two-step reaction: first oxidation to the corresponding dipyrrin using 2,3-dicloro-5,6-dicyano-1,4-benzoquinone and subsequent complexation with boron upon treatment with boron trifluoride etherate ($BF_3{\cdot}Et_2O$) in the presence of triethylamine (35% yield; Scheme 1).[60] Reactions of the ligand **L1** with chloro-bridged dimeric precursors $[(phpy)_2Ir(\mu\text{-}Cl)]_2$ and $[\{(\eta^5\text{-}C_5Me_5)Ir(\mu\text{-}Cl)Cl\}_2]$ in dichloromethane/methanol (1:1) under stirring conditions (room temperature, 16 h) afforded cationic complexes **1** and **2** in good yield (70−80%). These were isolated as their hexafluorophosphate salt by adding a saturated solution of NH_4PF_6 in methanol. A simple synthetic strategy adopted for the preparation of **A**, **B**, ligand **L1**, and complexes **1** and **2** is shown in Scheme 1.

The complexes under study are unaffected by air and moisture, soluble in common organic solvents like methanol, ethanol, acetone, dimethylformamide, dimethyl sulfoxide

DOI: 10.1021/acs.inorgchem.7b01693
Inorg. Chem. XXXX, XXX, XXX−XXX

Table 1. Crystal Data and Structure Refinement Parameters for L1, 1, and 2

crystal param	L1	1	2
empirical formula	$C_{66}H_{47}B_3F_6N_{15}O_3$	$C_{44}H_{32}BF_8IrN_7OP$	$C_{32}H_{31}BClF_8IrN_5OP$
fw	1244.61	1061.20	923.05
cryst syst	triclinic	monoclinic	triclinic
space group	$P\bar{1}$	$C2/c$	$P\bar{1}$
a (Å)	10.9626(3)	24.3469(5)	10.0848(3)
b (Å)	15.8202(4)	15.2786(3)	11.5614(4)
c (Å)	18.2066(6)	26.9194(5)	17.1320(4)
α (deg)	109.971(3)	90.00	95.205(2)
β (deg)	97.368(2)	102.173(2)	91.872(2)
γ (deg)	94.100(2)	90.00	99.623(2)
V (Å^3)	2920.59(2)	9788.5(3)	1958.94(1)
color and habit	red, needle	red, block	red, block
Z	2	4	2
d_{calcd} (g cm^{-3})	1.415	1.562	1.565
temperature (K)	293(2)	150(2)	293(2)
wavelength (Å)	1.54184	0.71073	1.54184
μ (mm^{-1})	0.862	2.830	8.230
GOF on F^2	1.033	1.090	1.046
R indices (all data)	R1 = 0.0556, wR2 = 0.1573	R1 = 0.0532, wR2 = 0.1472	R1 = 0.0584, wR2 = 0.1643
final R indices [$I > 2\sigma(I)$]	R1 = 0.0673, wR2 = 0.1677	R1 = 0.0758, wR2 = 0.1734	R1 = 0.0601, wR2 = 0.1676

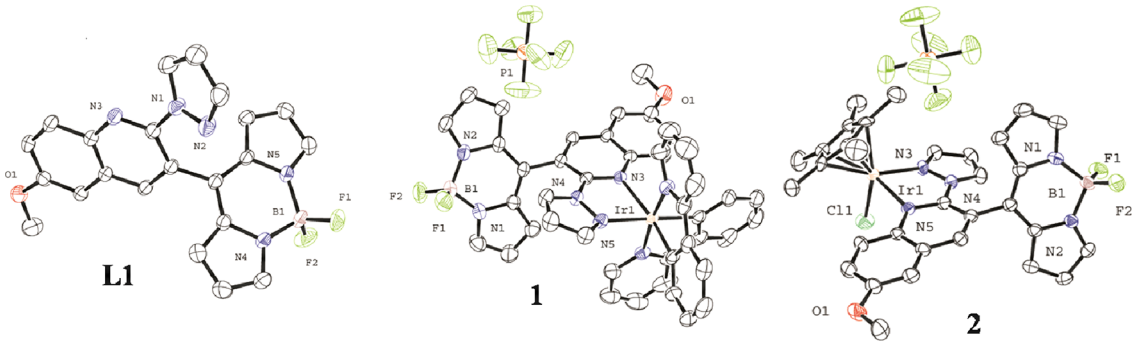

Figure 1. ORTEP views of L1, 1, and 2 at 30% thermal ellipsoid probability (H atoms are omitted for clarity).

(DMSO), acetonitrile, dichloromethane, chloroform, and water, and insoluble in diethyl ether, hexane, and petroleum ether. These have been meticulously characterized by satisfactory elemental analyses and spectroscopic studies [electrospray ionization mass spectrometry (ESI-MS), ^{1}H and ^{13}C NMR, UV/vis, and fluorescence]. Crystal structures of **L1**, **1**, and **2** have been determined by single-crystal X-ray analyses. Structures of **1** and **2** have also been optimized theoretically using geometrical coordinates from their crystallographic data.

NMR Spectral Studies. To affirm the formula, purity, and integrity of these compounds, ^{1}H and ^{13}C NMR spectra have been acquired in $CDCl_3$ at room temperature. The resulting data are summarized in the Experimental Section and the spectra depicted in Figures S1–S4. ^{1}H NMR spectra of **B** display peaks due to methoxy (δ 3.87), *meso* (δ 6.29), pyrrolic [δ 5.89, 6.11, 6.70, and 9.07 (br, N*H*)], aromatic and pyrazole protons (δ 6.46, 6.99, 7.33, 7.79, 7.88, 8.15, and 8.19). ^{1}H NMR spectra of **L1** show a loss of the resonances due to *meso*-subsituted −C*H* and −N*H* protons, which suggests its oxidation and subsequent complexation with the boron center. The pyrrolic and aromatic protons resonate at their usual positions with a small downfield shift.[61] ^{1}H NMR spectra of **1** and **2** display resonances due to BODIPY protons as well as signals associated with precursor complexes. After complexation with $[(phpy)_2Ir(\mu\text{-}Cl)]_2$ and $[\{(\eta^5\text{-}C_5Me_5)Ir(\mu\text{-}Cl)Cl\}_2]$, the BODIPY proton resonances exhibit a downfield shift relative to free BODIPY. Moreover, protons due to the metal precursor exhibit an upfield shift in the complexes relative to precursors $[\{(phpy)_2Ir(\mu\text{-}Cl)\}_2]$ and $\{(\eta^5\text{-}C_5Me_5)Ir(\mu\text{-}Cl)Cl\}_2]$. The relative shifts and intensities of the ligand and η^5-bonded hydrocarbon protons affirm the coordination of BODIPY with the metal center and formation of the complexes. In an analogous manner, ^{13}C NMR spectral data of **1**–**2** further support the formation of these complexes.

Mass Spectral Studies. The composition and stability of **L1** and complexes **1** and **2** were investigated by ESI-MS (Figure S5). In its mass spectrum, **L1** displays a molecular ion peak at m/z 438.1351 (calcd m/z 438.1314) due to $(M + Na)^+$. Complexes **1** and **2** exhibit molecular ion peaks at m/z 937.1200 (calcd m/z 937.1000) due to $(M - PF_6)^+$ and m/z 778.2 (calcd m/z 778.1) due to $(M - PF_6)^+$, respectively, arising as a result of loss of the counteranion hexafluorophosphate. Further, formulation of the ligand and complexes has been verified by determination of their crystal structures.

Crystal Structures. The structures of **L1**, **1**, and **2** have been determined by single-crystal X-ray analyses. Details about data collection, solution, and refinement are given in the Experimental Section and Table 1. The ligand **L1** crystallizes in a triclinic system with the space group $P\bar{1}$. The B atom lies within the dipyrrin plane and adopts the usual tetrahedral

DOI: 10.1021/acs.inorgchem.7b01693
Inorg. Chem. XXXX, XXX, XXX−XXX

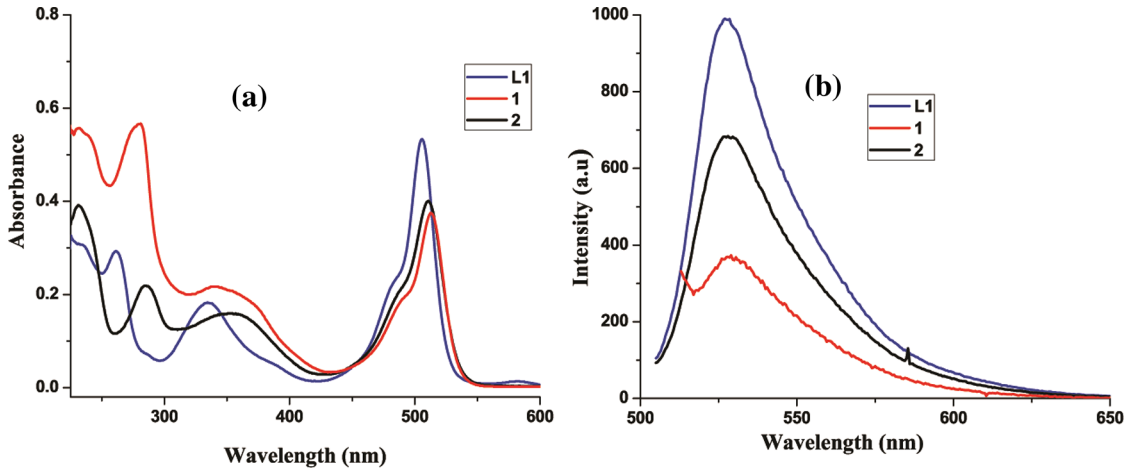

Figure 2. UV/vis (a) and fluorescence (b) spectra of **L1** and complexes **1** and **2** in PBS (*c*, 10 μM, pH ~ 7.4).

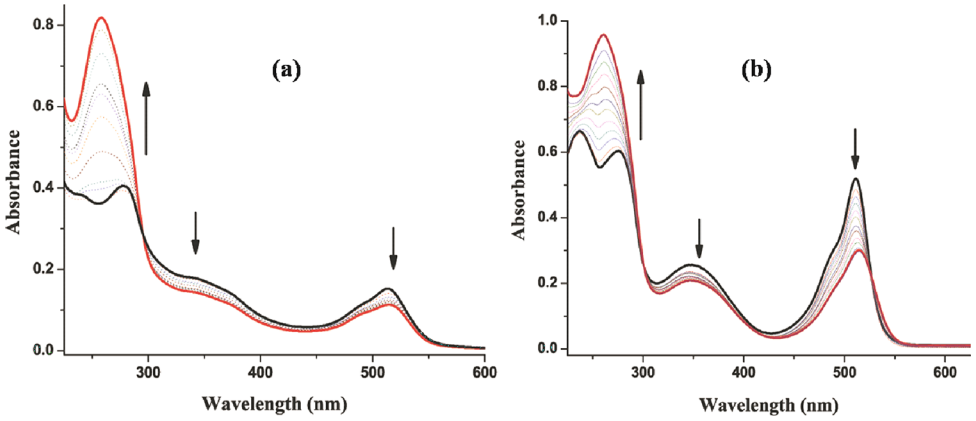

Figure 3. UV/vis spectra of **1** (a) and **2** (b) in PBS with increasing concentrations of CT-DNA (0–20 μM) at room temperature. Arrows show absorbance changes with increasing CT-DNA concentration.

geometry. Angles N–B–N and F–B–F are 106.26° and 110.14°, respectively, and are comparable to those of other related systems.[61] The dihedral angle between boron dipyrrin units and the quinoline ring (C4–C5–C11–C12) is 66.00°. Complex **1** crystallizes in the monoclinic system with the space group *C*2/*c*, while **2** is in the triclinic system with the space group $P\bar{1}$. Their pertinent view along with partial atomic numbering scheme is depicted in Figure 1, and important geometrical parameters are summarized in Table 1.

The crystal structure of **1** showed that the [$(phpy)_2$Ir] unit is coordinated with a N^N-chelating site of the BODIPY moiety, creating a slightly distorted octahedral geometry about the Ir metal center. The N3–Ir1–N5, N6–Ir1–C44 and N7–Ir1–C42 bite angles in this complex are 74.3(3)°, 80.6(4)°, and 80.4(4)°, respectively. The N6 and N7 atoms from 2-phenylpyridine are trans-disposed, which is normal and similar to earlier reports.[62−65] The Ir1–C and Ir1–N bond distances [Ir–C, 2.00 Å; Ir–N, 2.04 Å] and C–Ir1–N, C–Ir1–C, and N–Ir1–N bond angles are regular and similar to other closely related cyclometalated iridium(III) complexes.[22,46,62,63,65] On the other hand, Ir1 in complex **2** adopted the typical "piano-stool" geometry, wherein the metal center coordinated with the C_5Me_5 ring in an η^5-fashion, occupying three coordination sites. Other sites about the metal center are occupied by the N^N-chelating site of BODIPY via N3 and N5 atoms and a chloro group. The Ir–N and Ir–Cl bond distances [Ir–N3, 2.08 Å; Ir–N5, 2.15 Å; Ir–Cl1, 2.38 Å] in this complex are normal and comparable to those of other related systems.[11,12,53] The N–Ir–N and N–Ir–Cl angles are close to 90° [N3–Ir–N5, 74.29°; N3–Ir–Cl1, 87.85°; N5–Ir–Cl1, 87.15°] (Table S1). The η^5-C_5Me_5 ring is symmetrically bonded to the metal center with an average Ir–C distance of 2.14 Å (range 2.12–2.16 Å). All of the C atoms in the η^5-C_5Me_5 ring are planar, and iridium is displaced from the centroid of the ring by 1.78 Å, which is consistent with other reported iridium complexes.[11,12,53]

Electronic Absorption Spectroscopy. UV/vis absorption spectra of **L1**, **1**, and **2** have been acquired in phosphate-buffered saline (PBS; *c*, 10 μM; pH ~ 7.4) at room temperature (Figure 2a). Spectra of these compounds display strong low-energy absorptions at ~505 nm [504 nm, **L1**; 510 nm, **1**; 514 nm, **2**] and weak bands at ~480 nm [480 nm, **L1**; 484 nm, **1**; 488, nm **2**]. These have been attributed to S0–S1 and S0–S2 transitions of the conjugated dipyrrinato ligand.[53,58,66] Also, spectra of the compounds display intense high-energy bands at ~335 nm [335 nm, **L1**; 343 nm, **1**; 355 nm, **2**] due to intraligand π–π^* transitions.

Ligand **L1** and complexes **1** and **2** are luminescent in a buffer solution (PBS, pH ~ 7.4), and all of the photophysical experiments were performed in this system. Upon excitation at their respective λ_{ex} values (**L1**, 500 nm; **1**, 505 nm; **2**, 510 nm) in 100% PBS (Figure 2b), these showed emission maxima at similar positions of ~525 nm (**L1**, 520 nm; **1**, 525 nm; **2**, 530

DOI: 10.1021/acs.inorgchem.7b01693
Inorg. Chem. XXXX, XXX, XXX–XXX

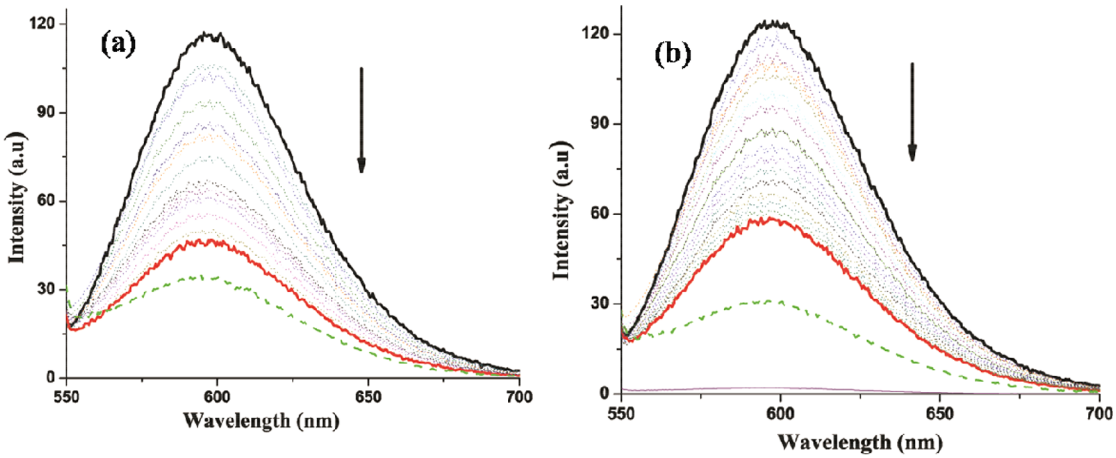

Figure 4. Emission spectra of EB bound to DNA in the absence (--- green line) and presence of **1** (a) and **2** (b). [EB] = 10 μM; [DNA] = 100 μM; [**1**] and [**2**] = 0−50 μM. Arrows show changes in the emission intensity upon the addition of increasing concentrations of the complexes.

nm).[66−68] As a consequence of complexation, emission maxima for **1** and **2** showed a red shift of ∼10 nm relative to ligand **L1**.

Electronic Absorption Titration Studies. Absorption titration studies have been carried out (Figure 3) using a fixed concentration of **1** and **2** (10 μM) and an increasing amount of calf-thymus DNA (CT-DNA; 0−20 μM). Usually, intercalation or interaction of the metal complexes with base pairs of DNA causes hypochromism with a small red/blue shift, while the hyperchromic shift arises because of nonintercalative/electrostatic interactions.[57,58,69−72] The extent of hypochromism gives an idea about the strength of the intercalative binding interaction. The band at 512 nm for **1** displays hypochromism (35%) with a small red shift of 5 nm upon the addition of CT-DNA, while the weak band at 278 nm shows hyperchromism (50%) along with a red shift of 20 nm. This indicates that interaction with the DNA results in the formation of a DNA−drug complex, causing stabilization of the DNA duplex.[53,57,58,69−72] Similarly, the gradual addition of CT-DNA to a solution of **2** led to hypochromism (33%) for the band at 510 nm with a small red shift of 4 nm. In addition, the band due to the intraligand charge-transfer transition at 276 nm displays hyperchromism (37%) with a blue shift of 16 nm. The hyperchromic effect may arise because of electrostatic attraction between a charged cation and the phosphate group of the DNA backbone, which may cause contraction and overall damage to the DNA secondary structure. Observed spectral changes clearly indicated that **1** and **2** interact with DNA through intercalation as well as groove binding via electrostatic interactions, leading to DNA stabilization.[53,57,58,69−72]

To compare their DNA binding affinity, the intrinsic binding constant K_b was calculated using the equation[69,73]

$$[\mathrm{DNA}]/(\varepsilon_a - \varepsilon_f)/ = [\mathrm{DNA}]/(\varepsilon_b - \varepsilon_f) + 1/k_b(\varepsilon_b - \varepsilon_f) \quad (1)$$

where [DNA] is the concentration of DNA in base pairs, ε_a is the apparent extinction coefficient, calculated as A_{obs}/[complex], and ε_f and ε_b are to the extinction coefficients of the complex in its free and bound forms, respectively. Each set of data upon fitting in the above equation gave a straight line with a slope of $1/(\varepsilon_b - \varepsilon_f)$ and a y intercept of $1/K_b(\varepsilon_b - \varepsilon_f)$. K_b was determined from the ratio of te slope to the intercept (Figure S7a). The values of K_b vary in the order **1** (5.8×10^4) > **2** (4.7×10^4).

Ethidium Bromide (EB) Displacement Studies. To understand the binding mode of the compounds with DNA, competitive binding studies have been carried out between EB (3,8-diamino-5-ethyl-6-phenylphenanthridine bromide) and **1** and **2** with CT-DNA.[74,75] EB is an intercalating weakly fluorescent labeling agent often used for staining nucleic acid and other biomolecules.[57,58,69−72,76] After binding with DNA, its fluorescence intensity increases and displacement of EB (λ_{ex}, 540 nm; λ_{em}, 600 nm) from an EB−DNA complex by other compounds causes quenching of intrinsic fluorescence of the EB−DNA system. This occurs because of an increase in the concentration of free EB in solution and a lowering of the number of binding sites accessible for EB−DNA binding.

The effects of **1** and **2** on the fluorescence intensity of the EB−DNA system are shown in Figure 4. Notably, the fluorescence intensity of EB−DNA underwent an appreciable decrease (60%, **1**; 54%, **2**) in the presence of **1** and **2** (50 μM) with increasing concentrations. It has been concluded that **1** and **2** are capable of displacing EB from the EB−DNA complex and strongly interact with DNA binding sites in the order **1** > **2**. The quenching parameters were analyzed using the Stern−Volmer equation (Figure S7b)

$$I_0/I = K_q[\mathrm{Q}] + 1 \quad (2)$$

where I_0 is the emission intensity in the absence of the quencher, I is the emission intensity in the presence of the quencher, K_q is the quenching constant, and [Q] presents the concentration of the complex (Q = quencher). K_q values have been derived from the slope of I_0/I versus [Q] plot (2.25×10^4, **1**; 2.08×10^4, **2**). Additionally, the apparent DNA binding constants (K_{app}) were calculated using the equation

$$K_{EB}[\mathrm{EB}] = K_{app}[\mathrm{complex}] \quad (3)$$

where [complex] is the value at a 50% decrease of the fluorescence intensity for EB, K_{EB} (4.94×10^5 M^{-1}) is the DNA binding constant for EB, and [EB] is the concentration of EB (10 μM). K_{app} values were found to be 3.18×10^5 M^{-1} (**1**) and 2.64×10^5 M^{-1} (**2**). This suggests that complex **1** intercalated rather strongly relative to **2**, and this observation is in good agreement with the conclusions drawn from UV/vis titration studies.

Protein Binding Studies. Fluorescence spectroscopy is very useful in investigating the interaction and mechanism of

DOI: 10.1021/acs.inorgchem.7b01693
Inorg. Chem. XXXX, XXX, XXX−XXX

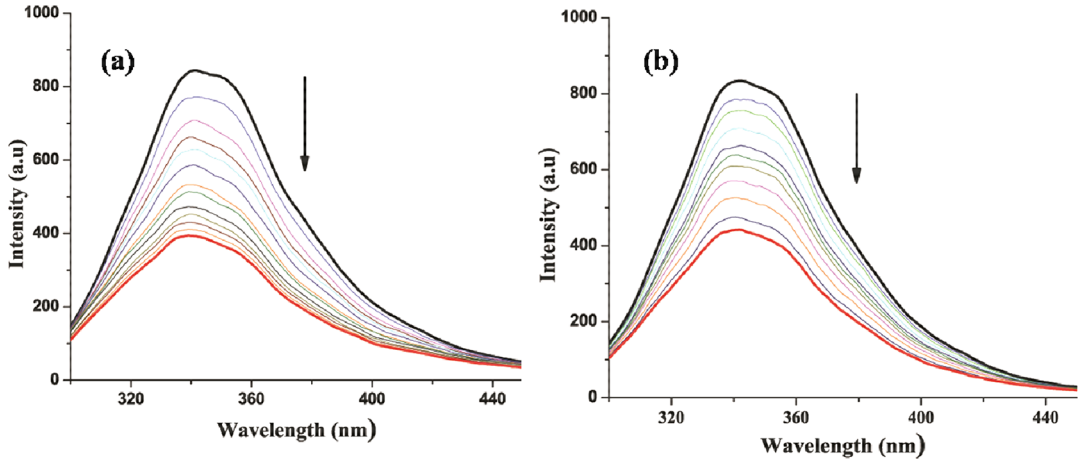

Figure 5. Emission spectrum of BSA (0.5 μM; λ_{ex} = 280 nm; λ_{em} = 343 nm) in the presence of increasing amounts of **1** (a) and **2** (b) (0−50 μM). Arrows show that the emission intensity changes with increasing concentration of the complexes.

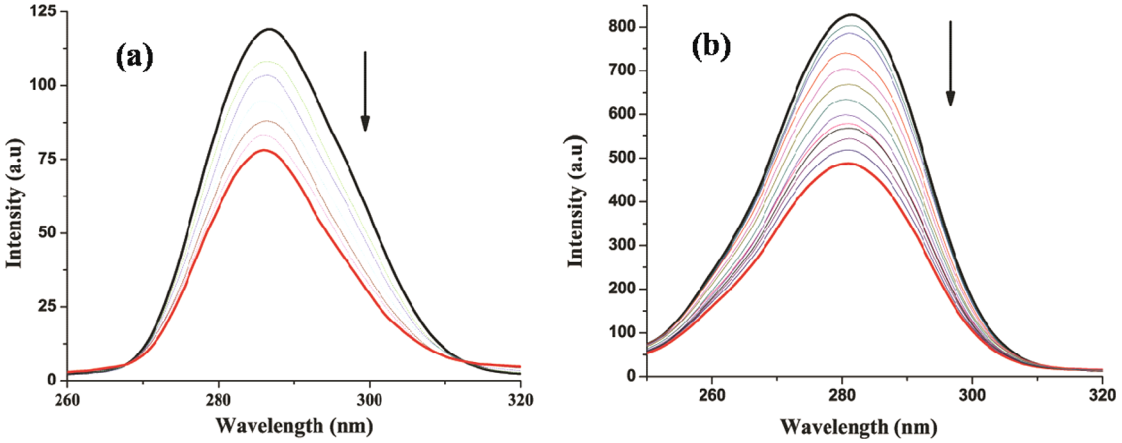

Figure 6. Synchronous spectra of BSA (black line; PBS buffer, *c*, 0.5 μM, pH ~ 7.4) in the presence (other lines) of increasing amounts (0−50 μM) of **1** at wavelength differences of (a) $\Delta\lambda$ = 15 nm and (b) $\Delta\lambda$ = 60 nm. Arrows show decreases in the emission intensity with increasing concentrations.

binding of the compounds with bovine serum albumin (BSA).[35,58,77−79] For this purpose, BSA is preferred over other proteins because of its abundance, cost effectiveness, ease of purification, stability, and wide applications.[35,58,77−79] It has been established that the high fluorescent nature of BSA is due to tryptophan and tyrosine residues.[35,58,77−79] Quenching of the emission intensity of BSA may occur in the presence of the complexes because of changes in the secondary structure of protein induced by various molecular interactions.[57,80,81] Fluorescence quenching experiments on BSA in the presence of complexes provide useful information about the structure, dynamics, and protein folding.[35,58,77−82] Fluorescence changes (range 290−500 nm; λ_{ex}, 280 nm) in the spectrum of BSA in the presence of varying amounts of **1** and **2** (0−50 μM) are depicted in Figure 5. The intensity of the fluorescence band for BSA at ~345 nm is quenched (58%, **1**; 52%, **2**) relative to its initial intensity along with a small blue shift of ~5 and 4 nm upon the addition of **1** or **2**. From observations, we concluded that some interaction is certainly taking place between the complexes and BSA. One can get an idea about the structural changes and the types of quenching (static or dynamic) from the UV/vis study (Figure S9). It is well documented that dynamic quenching absorption spectra of fluorophore do not show a substantial change, while static quenching causes perturbation in the absence and presence of the compounds.[35,57,77−79]

From Figure S9, it is clear that the addition of **1** and **2** to a fixed concentration of BSA leads to an increase in the intensity (λ_{abs} = 220 nm), with a small blue shift indicating that these complexes interact with the protein and follow a static quenching mechanism. Fluorescence quenching data have been analyzed using the Stern−Volmer (Figure S10a) and Scatchard equations and quenching constant (K_q) evaluated from the plot of I_0/I versus [Q]. The equilibrium binding constant can be estimated from the Scatchard equation:

$$\log[(I_0 - I)/I] = \log K_{bin} + n \log [Q] \quad (4)$$

where K_{bin} is the binding constant of the compound with BSA and n is the number of binding sites. From the $\log[(I_0 - I)/I]$ vs log [Q] plot, the number of binding sites (n) and the binding constant (K_{bin}) have been calculated (Table S2). Notably, estimated values of n for these compounds are ~1 and strongly suggest the presence of a single binding site in BSA for **1** and **2**. The values of K_q and K_{bin} for these compounds further suggest that **1** interacts with BSA rather strongly relative to **2**.

Synchronous Fluorescence Experiments. Valuable information about the microenvironment around the fluorophore can be obtained from synchronous fluorescence

DOI: 10.1021/acs.inorgchem.7b01693
Inorg. Chem. XXXX, XXX, XXX−XXX

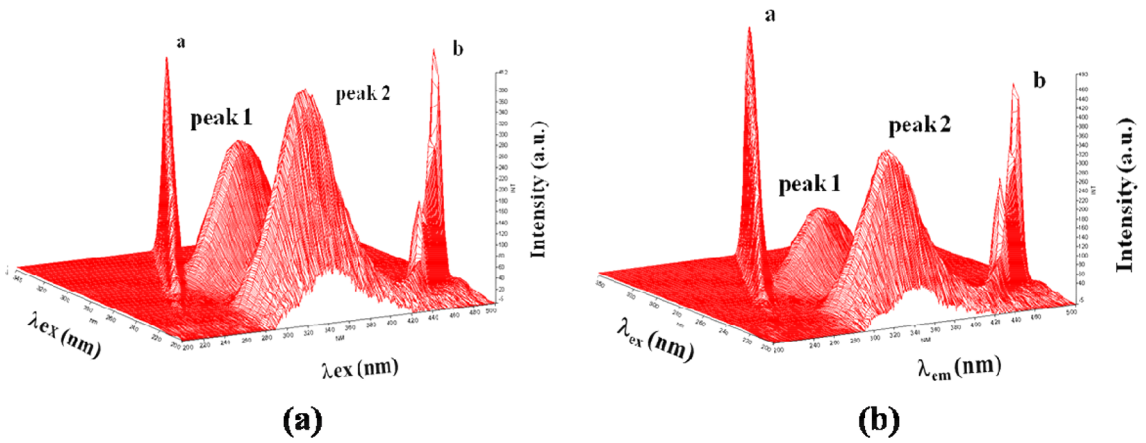

Figure 7. 3D fluorescence spectra of BSA (a) and BSA + **1** (b). [BSA] = 10^{-6} mol L^{-1}; [**1**] = 10^{-5} mol L^{-1}.

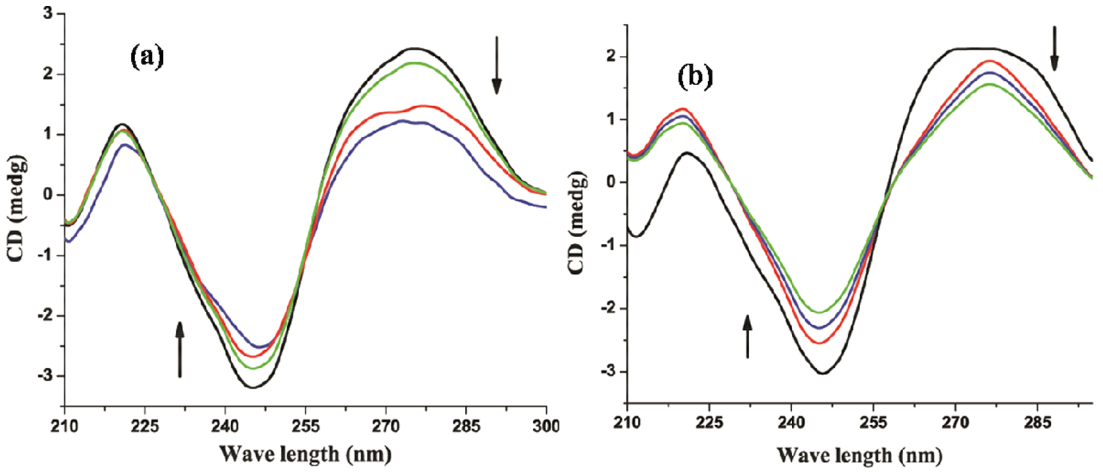

Figure 8. CD spectra of CT-DNA in the absence and presence of complexes **1**(a) and **2** (b). [DNA] = 100 μM; [complex] = 0−50 μM.

spectroscopy.[35,58,83,84] To investigate conformational changes in BSA in the presence of **1** and **2**, fluorescence spectroscopic experiments were carried out at $\Delta\lambda$ = 15 and 60 nm ($\Delta\lambda = \lambda_{ex} - \lambda_{em}$). A larger wavelength difference ($\Delta\lambda$ = 60 nm) provides information about the microenvironment for tryptophan and a shorter one ($\Delta\lambda$ = 15 nm) that for the tyrosine residue.[70,77,84] Emission maxima of tryptophan and tyrosine residue in proteins depend on the polarity of its surroundings.

It has been observed that synchronous fluorescence spectra ($\Delta\lambda$ = 15 nm) for BSA with increasing concentrations of **1** and **2** exhibit a significant decrease in the intensity for the band at 288 nm (35.85%, **1**; 31.55%, **2**) without any noticeable shift (Figures 6 and S8). On the other hand, at $\Delta\lambda$ = 60 nm, they showed a remarkable decrease in the fluorescence intensity for the band at 280 nm (87.42%, **1**; 86.82%, **2**) with small blue shifts of 3 and 4 nm. This suggests that the fluorescence intensities for both tryptophan and tyrosine diminished with increasing concentrations of the complexes.[57,58,70,77,84] It further supported that the hydrophobicity around both the tyrosine and tryptophan residues increases and the polarity decreases.

Three-Dimensional (3D) Fluorescence Spectroscopy. Excitation−emission matrix or 3D fluorescence spectroscopy provides useful information about the emission characteristics of the fluorophore by changing the excitation and emission wavelengths simultaneously.[85,86] Using this technique, one can have an idea about the conformational and microenvironmental changes for BSA in the presence of the complexes.[57,58,85,86] Spectral changes arising for BSA in the presence of **1** and **2** are depicted in Figures 7 and S11. Notably, the 3D spectrum of BSA exhibits four characteristic peaks: a peak on the extreme left, namely, peak 'a' assigned as the first-order Rayleigh scattering for which the emission wavelength matches the excitation wavelength ($\lambda_{ex} = \lambda_{em}$), and the peak on the extreme right designated as peak 'b' ascribed to the second-order Rayleigh scattering for which $\lambda_{em} = 2\lambda_{ex}$. In addition, peak 1 is characteristic of the tyrosine and tryptophan residues, and peak 2 is related to the polypeptide backbone and secondary structure of the protein.[57,58,85,86]

The fluorescence intensity for peak 1 quenched in the presence of complexes **1** and **2** (peak 1: 24.4%, **1**; 18.0%, **2**), suggesting their binding with BSA and closeness of the binding sites to the tryptophan and tyrosine residues. Peak 2 also exhibited quenching (27.9%, **1**; 22.2%, **2**) and suggested changes in the peptide structure of BSA. From the 3D and synchronous fluorescence spectral studies, we conclude that interaction between BSA and **1** and **2** may be due to the unfolding of the polypeptide and conformational changes in the protein due to enhanced exposure to the hydrophobic region.

Circular Dichroism (CD) Spectroscopy. The conformational changes caused by **1** and **2** in CT-DNA have been monitored by CD spectroscopic studies in a PBS buffer at room temperature (Figure 8). CT-DNA itself shows bands at (−) 245 and (+) 275 nm assignable to the right-handed helicity of

DOI: 10.1021/acs.inorgchem.7b01693
Inorg. Chem. XXXX, XXX, XXX−XXX

B-DNA and base-pair stacking.[87,88] Interaction of non-intercalative drugs with DNA causes negligible perturbation for the bands due to base stacking and helicity, whereas an intercalator leads to changes in the intensity of both bands. Further, these are sensitive toward the binding of small molecules and a drug.[70,87−89] An increase in the concentrations of **1** and **2** led to a decrease in the intensity for both (+) and (−) bands due to CT-DNA, which clearly indicated interaction between the complexes and CT-DNA.

From this data, we conclude that **1** and **2** may intercalate between neighboring base pairs of CT-DNA mainly because of the presence of a planar aromatic dipyrrin moiety. Further, the intensity change follows the order **1** > **2**, indicating greater efficacy of **1** relative to **2** which is consistent with the UV/vis and fluorescence spectroscopic studies.

Viscosity Measurements. To understand the nature of the interaction between **1** and **2**, DNA viscosity measurements have been carried out in the absence and presence of varying concentrations of the complexes (Figure 9). Usually,

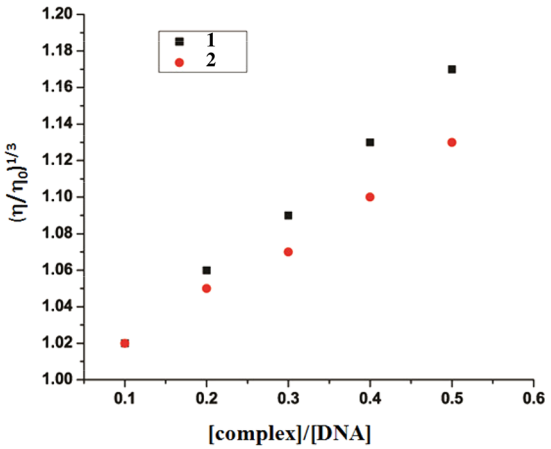

Figure 9. Effect of increasing amounts of complexes on the relative viscosity of CT-DNA (125 μM) in a PBS buffer at 25 °C in various [complex]/[DNA] ratios.

intercalators elongate the DNA double helix by accommodating such molecules between the base pairs, leading to an increase in the viscosity.[52,90,91] In contrast, partial nonclassical intercalation leads to a bending (or a kink) in the DNA helix without altering its length and, thereby, viscosity.[92,93] A plot of the relative specific viscosity $(\eta/\eta_0)^{1/3}$ versus [complex]/[DNA] shows that the DNA viscosity significantly increases with an increase in the concentration of the complexes. On the basis of variation in the DNA viscosity, it has been concluded that complexes interact with CT-DNA in an intercalative mode.

Hydrolysis Study and Interaction with Nucleobases. Hydrolysis of the M−Cl bond represents an activation step for transition-metal anticancer complexes. M−OH_2 aqua complexes are typically more reactive relative to analogous chlorido complexes.[35−48] Hydrolysis of compound **2** in 5% CD_3CN/95% D_2O (v/v) was monitored by ^{1}H NMR spectroscopy at 298 K (Figure S6), and acetonitrile was used to ensure the solubility of complex **2** (the NMR spectrum of complex **2** in DMSO shows broad features). It (*c*, 1 mM) underwent rapid hydrolysis in 5% CD_3CN/95% D_2O within a minute, and the extent of hydrolysis for this complex is 52%. To further affirm hydrolysis of the complex, NaCl (4 mol equiv) was added to the equilibrium solution. ^{1}H NMR spectra was subsequently recorded within 10 min of the Cl^- addition at 298 K. Signals due to chlorido adducts enhanced in the intensity with the addition of NaCl, while those for the aqua forms decreased, suggesting a rapid shifting of the equilibrium toward chloride from the aqua complex and very fast aquation.

Partition Coefficient Determination. The partitioning behavior of the drugs is usually determined by the lipophilicity.[11,94−96] It has been worked out by measuring the partition coefficient (log *P*) based on the amounts of **1** and **2** distributed in a biphasic system (*n*-octanol/water) using the equation

$$\log P = \log [\text{complex}]_{\text{octanol}}/[\text{complex}]_{\text{water}} \quad (5)$$

Notably, calculated log *P* values (Table S3) are consistent with earlier reports.[19−35] Further, the log *P* value for **1** is greater relative to complex **2**, which may be related to the greater number of hydrophobic aromatic rings in it. These results are in keeping with 3-(4,5-dimethylthiazol-2-yl)-2,5-diphenyltetrazolium bromide (MTT) assay; the cytotoxicity of the complex increases with an increase in the lipophilicity.

Molecular Docking with DNA. To explore the most feasible binding site, interaction mode, and binding affinity, molecular docking studies have been carried out on **1** and **2** using B-DNA (PDB ID: 1BNA).[97] It is well-known that a DNA−intercalator complex stabilizes via van der Waals forces, hydrogen bonding, hydrophobic charge transfer, and electrostatic complementarities.[35,58,76,98,99]

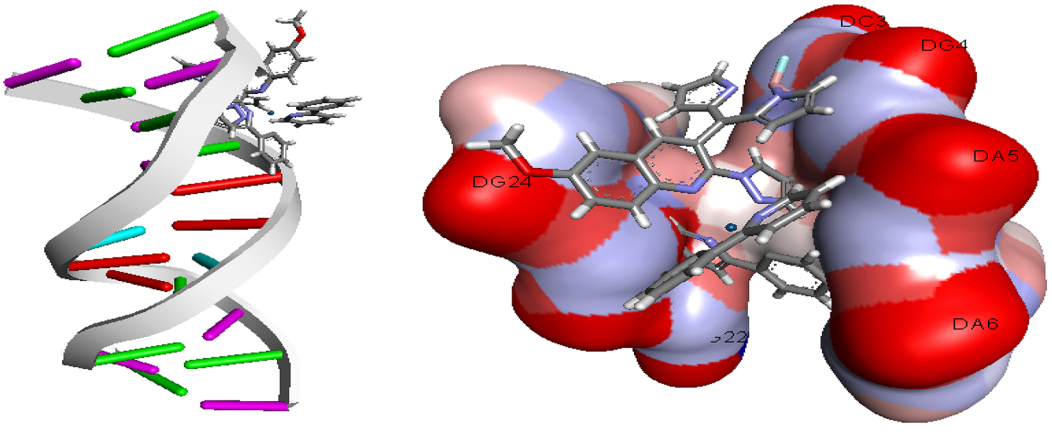

Figure 10. Docked model for **1** with DNA (PDB ID: 1BNA): open view (left); closed view (right).

DOI: 10.1021/acs.inorgchem.7b01693
Inorg. Chem. XXXX, XXX, XXX−XXX

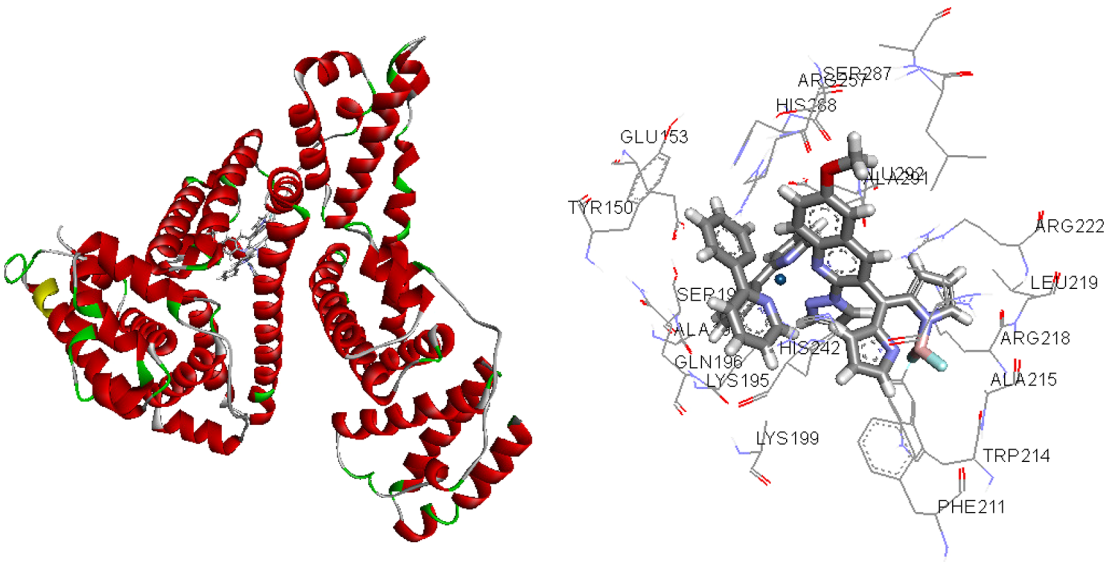

Figure 11. (left) Docked model of **1** located within the hydrophobic pocket of HSA (PDB ID: 1h9z). (right) Interaction mode between **1** and the polypeptide units.

The most stable binding conformation of **1** and DNA revealed that it stacks in minor grooves via electrostatic interactions and the complex is adjusted in such a way that a part of the planar dipyrrin core makes the stacking interaction favorable with DNA base pairs and fits inside the DNA strands by van der Waals forces and hydrophobic contacts (Figures 10 and S14).[27,80] The resulting relative binding energies for docked structures of **1** and **2** have been found to be −285.75 and −277.11 eV, respectively, which indicates the better binding capability of **1** relative to **2**. The results are consistent with UV/vis and competitive EB displacement studies.

Molecular Docking with Human Serum Albumin (HSA). To ascertain the binding mode and their location within the protein, molecular docking studies have been performed on complexes **1** and **2** with a protein (HSA).[35,57,58,100,101] HSA has been chosen over BSA for its structural homology, and it provides more biorelevant results. The 3D structure of crystalline albumin shows that it consists of three structurally homologous domains: I (residues 1−195), II (196−383), and III (384−585). Each domain has two subdomains: A and B. Figures 11 and S15 clearly indicate that the complexes are localized within the hydrophobic cavity of subdomain IIA. It has been discovered that the large hydrophobic cavity in subdomain IIA is capable of accommodating intercalator complexes. Amino acid residues around the binding sites are as follows: LYS199, TRP214, PHE211, ALA215, ARG218, LEU219, ARG257, SER287, HIS288, and ALA291 (**1**); LYS195, GLN196, LEU198, LYS199, SER202, PHE211, TRP214, ARG222, LEU238, HIS242, ARG257, ALA291, ASP451, SER454, and LEU481 (**2**) (within 4 Å; Table S4).

Docking studies further revealed the occurrence of various electrostatic and hydrogen-bonding interactions between the complexes and HSA. These interactions play a major role in lowering the hydrophilicity and enhancing the hydrophobicity of HSA and thereby stabilizing the complex·HSA system. The binding energies for the complexes with HSA are found to be −378.11 eV (**1**) and −321.58 eV (**2**) (Figures 11 and S15). The results also provided structural evidence for the distinct optical response of BSA in the presence of complexes **1** and **2**.

Density Functional Theory (DFT) Calculations. To understand the structure and verify the geometrical parameters (bond lengths and bond angles), geometry optimizations on **1** and **2** were carried out using the *Gaussian 09* package.[102] The Ir metal center was described by the LANL2DZ basis set, and the nonmetal atoms were described by the 6-31G** basis set.[103−106] The starting geometries were taken from the single-crystal X-ray data and subjected to optimization. Contour plots for the molecular orbitals were generated using *Gaussview 5.0*, and the energies of the frontier molecular orbitals for **1** and **2** were calculated. DFT calculations on **2** reproduced familiar three-legged "piano-stool" structures (Figure S12).

From DFT calculations, it is clear that the electron densities for both the highest occupied (HOMO) and lowest unoccupied (LUMO) molecular orbitals are localized mainly on the dipyrrin core of BODIPY and lack any electronic communication with the metal center (Figure S13). Calculated HOMO energies for the complexes are in the order **1** (−5.95 eV) > **2** (−6.07 eV), and those for the LUMO are **1** (−2.94 eV) > **2** (−3.02 eV). The differences between the HOMO and LUMO in **1** (−3.01 eV) and **2** (−3.04 eV) are almost identical. The higher HOMO energies for **1** relative to **2** are responsible for the better intercalative interaction between DNA base pairs and complex **1**.[69] The results are in good agreement with the experimental data, and factors like the lipophilicity, hydrogen bonding, steric bulk, rotational motion, etc., can also affect their biological activity.

Effect of L1, 1, and 2 on the Viability and Proliferation of the HeLa and Human Embryonic Kidney (HEK293) Cells. MTT assay has been performed to determine the cytotoxicity of ligand **L1** and complexes **1** and **2** in the concentration range of 20−100 μM.[107]

As depicted in Figure 12, **L1** displays marginal toxicity at relatively high concentrations (100 μM) after up to 24 h of treatment because more than 85% cells were found alive. On the other hand, **1** and **2** show relatively high toxicity, where approximately 26% and 29% cells were found alive. The estimated IC_{50} values for **1** and **2** turned out to be 32.4 and 51.9 μM, respectively, which are comparable to that of cisplatin

DOI: 10.1021/acs.inorgchem.7b01693
Inorg. Chem. XXXX, XXX, XXX−XXX

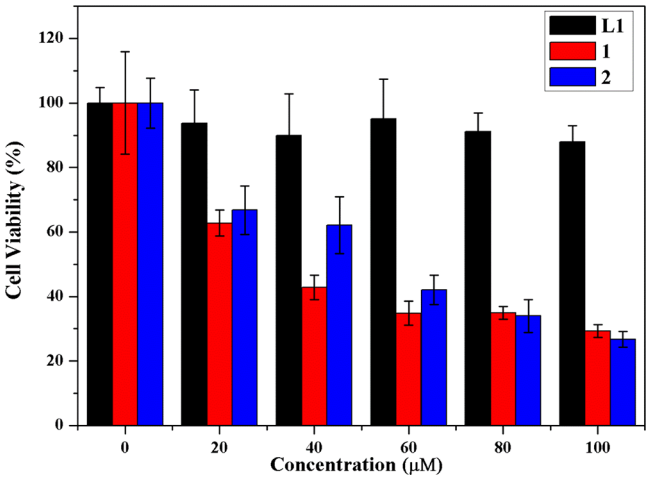

Figure 12. Cytotoxicity profile of **L1**, **1**, and **2** against the HeLa cell line.

(the calculated IC_{50} value under analogous conditions was found to be 21.6 μM). Further, to evaluate the selectivity of **1** and **2** toward cancer cells, a cytotoxicity experiment was also carried out against normal cell lines, HEK293. As shown in Figure S17, **1** and **2** show less toxicity toward HEK293 cells than HeLa cells. The estimated IC_{50} values for **1** and **2** turned out to be 85.5 and 100 μM, respectively. Under similar conditions, cisplatin showed IC_{50} of 80.1 μM, indicating the selectivity of **1** and **2** toward cancer cells is comparable to that of cisplatin. In summary, **1** elicited a maximum toxicity response, followed by **2** for both cell lines.

Change in the Nuclear Morphology and Apoptosis Induction. The nuclear morphology is a powerful indicator of cellular health and apoptotic conditions; hence, changes in the nuclear morphology following treatment with **1** and **2** have been examined by Hoechst 33342 staining.[69,108,109] Changes in the nuclear morphology, chromatin condensation, and fragmented nuclei are a few characteristics of apoptotic cells. As shown in Figure 13, the cells treated with **1** and **2** show uneven nuclear staining, and abnormal nuclear morphology along with condensed chromatin, as shown by bright spots within the nuclei. This clearly indicates apoptotic efficacy of **1** and **2**, leading to cancer cell death.

In Vitro Confocal Microscopic Experiments. The detection of **L1** and complexes **1** and **2** in living cells has also been explored by fluorescence microscopy. The complexes were incubated with HeLa cells for 2 h at 37 °C and visualized by a confocal fluorescence microscope. As shown in Figure 14, **L1**, **1**, and **2** enter the cell membrane and show significant intracellular fluorescence. A closer observation revealed that **L1** and **1** show distinct fluorescence in the extranuclear region with a clear demarcation of the nuclear membrane, while **2** distributed unevenly throughout the cell. Moreover, major differences were not observed between the BODIPY ligand and its metal derivatives, implying that uptake and distribution characteristics of the compounds are mainly determined by the BODIPY moiety.

CONCLUSION

In summary, through this work, two iridium(III) complexes containing a BODIPY ligand have been synthesized and thoroughly characterized by various techniques. It has been clearly shown that these efficiently interact with DNA in an intercalative mode. From the molecular docking studies, it has been established that **1** and **2** bind with DNA in its minor groove via intercalative interactions but with protein via hydrophobic residues located within the subdomain IIA cavity. Indeed, the fluorescence characteristics of the ligand and complexes allowed monitoring of their in vitro uptake in cancer cells. These exhibited significant cytotoxicity toward the HeLa cell line and showed a preference for accumulation in cell membranes without reaching the nuclei. Moreover, it is apparent that the BODIPY moiety solely determines the cellular uptake and fluorescence staining pattern of the ligand and complexes. Among these, **1** displayed the lowest IC_{50} value and distinct changes in the nuclear morphology, with fragmented nuclei on the cell surface indicating apoptotic cell death. Correlation analysis showed that an increase in the hydrophobicity of **1** causes an increase in cellular accumulation, which generally results in an increase in the potency. The results shown here will be helpful in understanding the interaction of iridium complexes with DNA and proteins. Importantly, it also highlights that inclusion of 2-phenylpyridine along with N^N-donor ligand can create complexes with enhanced potency and thereby provide a new strategy beneficial for the development of these types of complexes.

EXPERIMENTAL SECTION

Reagents. Standard literature procedures have been employed for drying and distilling the solvents prior to their use.[110] Hydrated iridium(III) chloride, 2-phenylpyridine, pentamethylcyclopentadiene, 2,3-dicloro-5,6-dicyano-1,4-benzoquinone (DDQ), pyrrole, trifluoroacetic acid, anisidine, triethylamine, and boron trifluoride diethyl etherate were procured from Sigma-Aldrich India and used as received without further purification. 3-(4,5-Dimethylthiazol-2-yl)-2,5-diphenyltetrazolium bromide (MTT) and ethidium bromide (EB) were

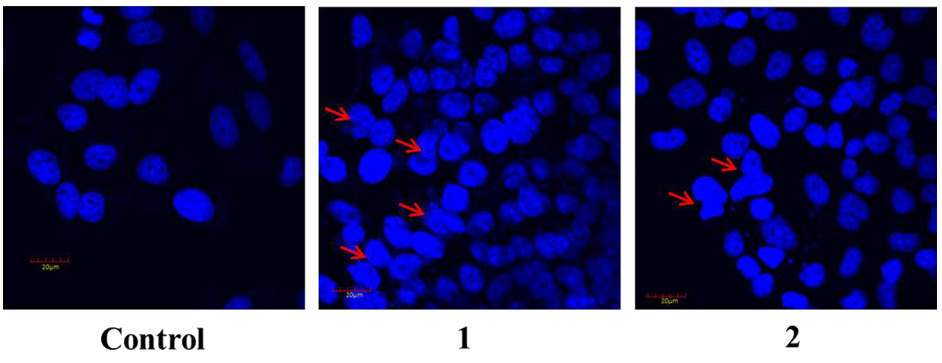

Figure 13. Nuclear morphology using Hoechst staining following treatment with **1** and **2** (scale bar: 20 μm).

DOI: 10.1021/acs.inorgchem.7b01693
Inorg. Chem. XXXX, XXX, XXX−XXX

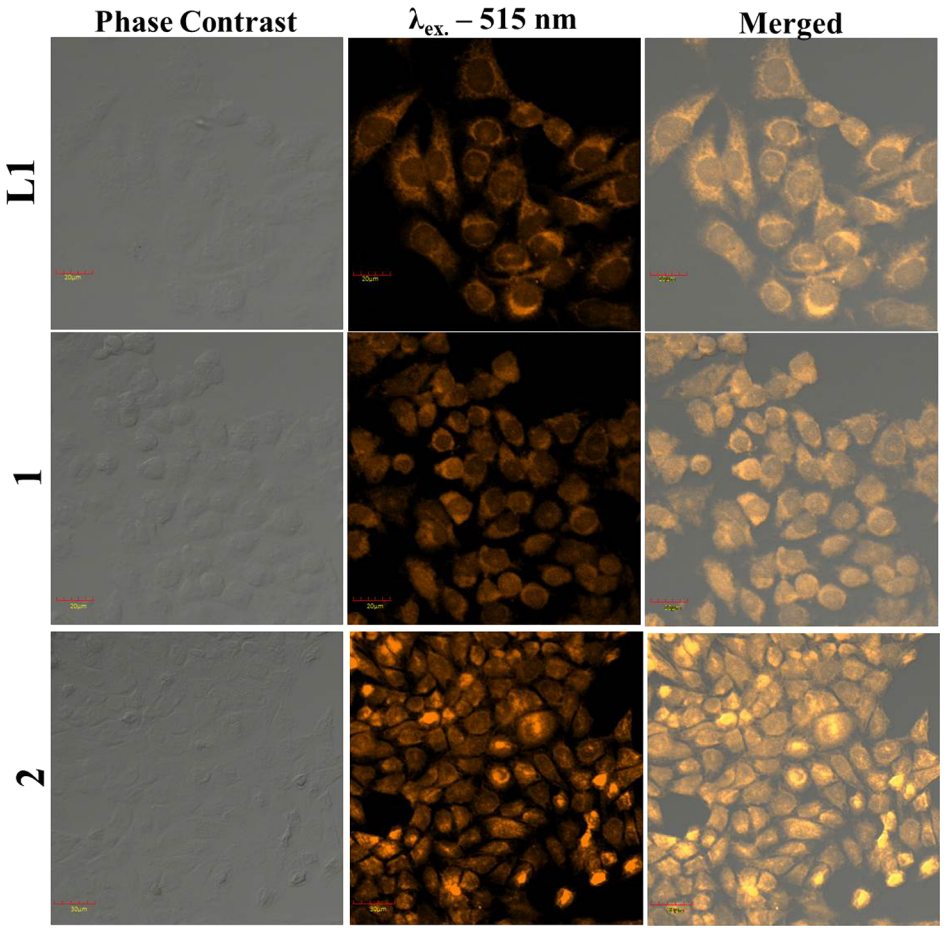

Figure 14. Cellular uptake of **L1**, **1**, and **2** by HeLa cell lines (scale bar: 20 μm).

purchased from Hi-Media Laboratories and Loba Chemie, respectively. Calf-thymus DNA (CT-DNA) was acquired from Bangalore Genei. Human cervical cancer (HeLa) and human embryonic kidney (HEK293) cell lines were obtained from National Centre for Cell Science, Pune, India. Other common reagents of highest purity were purchased from local firms.

General Methods. Elemental analyses for C, H, and N were obtained on an Elementar Vario EL III Carlo Erba 1108 elemental analyzer. Electronic absorption and fluorescence spectra were acquired on Shimadzu UV-1601 and PerkinElmer LS 55 fluorescence spectrometers, respectively. ^{1}H and ^{13}C NMR spectra were acquired on a JEOL AL 500/300 FT-NMR spectrometer using tetramethylsilane [$Si(CH_3)_4$] as an internal reference. Electrospray ionization mass spectrometry (ESI-MS) measurements were made on a Bruker Daltonics Amazon SL ion-trap mass spectrometer. After dissolution of the samples in 100% acetonitrile with 0.1% formic acid, these were introduced into the ESI source through a syringe pump at a flow rate of 100 mL h^{-1}. The capillary voltage was 4500 V and dry gas flow 8 L min^{-1} with the dry gas at 300 °C. An MS scan was acquired for 2.0 min, and spectral printouts were averaged over each scan. Fluorescence microscopic images were taken on a EVOS FL cell imaging system.

X-ray Structure Determination. Crystals suitable for single-crystal X-ray analyses for **L1** and complexes **1** and **2** were obtained by the slow diffusion of hexane over a dichloromethane solution of the respective compounds. X-ray data were collected on a dual-source Supernova CCD system from Agilent Technologies (Oxford Diffraction) at room temperature with Mo Kα radiation (λ = 0.71073 Å). Structures were solved by direct methods (*SHELXS-97*) and refined by full-matrix least squares on F^2 (*SHELX-97*). All of the non-H atoms were treated anisotropically, and H atoms attached to C atoms were included as a fixed contribution and geometrically calculated and refined using the *SHELX* riding model.[111,112] The computer program *PLATON* was used for analysis of the interaction and stacking distances.[112−114] Disordered solvent molecules were removed by the *SQUEEZE* command in *PLATON*.[112−114] CCDC 1553126 (**L1**), 1553128 (**1**), and 1553125 (**2**) contain the supplementary crystallographic data for this paper.

Partition Coefficient Determination. The lipophilicities of **1** and **2** have been determined by the "shake-flask" method using octanol/water phase partitions. Octanol-saturated water and water-saturated octanol were prepared using analytical-grade octanol and double-distilled water. The complexes under study (1 mg mL^{-1}; 1:6 ethanol/water) were diluted to 2, 4, 6, 8, and 10 μg mL^{-1} in water; subsequently, these (1 mg mL^{-1}) were diluted to 2, 4, 6, 8, and 10 μg mL^{-1} in octanol. Appropriate amounts of the complexes (4 mg mL^{-1}) were shaken for 24 h at room temperature in equal volume (50:50). After equilibrium, the organic and aqueous phases were separated and centrifuged. Finally, the concentration of the drug in each phase was determined by UV/vis spectroscopy. The sample solution concentration was used to calculate log P and the partition coefficients for **1** and **2** using the equation log P = log $[\text{complex}]_{\text{octanol}}/[\text{complex}]_{\text{water}}$

Far-UV CD Spectroscopy. CD spectra were recorded on a Jasco J-815 spectropolarimeter at 25 °C using a quartz cell (0.1 cm path length) and scanned in the spectral range 220−300 nm. The concentration of CT-DNA (50 μM) was held constant and those for complexes **1** and **2** varied from 10 to 50 μM. The final spectra were taken as the average of two accumulated runs.

Viscosity Measurements. Viscosity measurements were made using an Ubbelodhe viscometer immersed in a constant-temperature bath at 25 °C. Data are presented as η/η_0 versus [complex]/[DNA], where η is the specific viscosity of DNA in the presence of complexes and η_0 is the specific viscosity of DNA alone in a PBS buffer. Specific

DOI: 10.1021/acs.inorgchem.7b01693
Inorg. Chem. XXXX, XXX, XXX−XXX

viscosity values have been calculated from the observed flow time of a DNA solution (t) corrected for the buffer alone (t_0), $\eta = (t - t_0)/t_0$.

Molecular Docking. Molecular docking studies on **1** and **2** have been performed using *HEX 6.1* software and *Q-SiteFinder*, an interactive molecular graphics program for interaction and docking calculations and to classify the possible binding sites of biomolecules.[98] DFT calculations have been carried out using *Gaussian 09* by the B3LYP method.[102] The geometries of the compounds have been optimized using a standard 6-31G** basis set for C, H, N, O, B, F, P, and Cl, while LANL2DZ was used for Ir with the effective core pseudopotential for the metal.[103−106] Coordinates for metal complexes have been taken from their optimized structures as a .mol file and transformed to PDB using *CHIMERA 1.5.1* software. The crystal structure of B-DNA (PDB ID: 1BNA) has been taken from the protein data bank (http://www.rcsb.org./pdb). Visualization of the docked molecules has been made by *Discovery Studio 3.5* software. The default parameters have been used for docking calculations with the correlation-type shape only, FFT mode at the 3D level, and grid dimension 6 with receptor range 180 and ligand range 180 with twist range 360 and distance range 40.

Preparation of the Stock Solutions of Ligands and Their Complexes. The complexes were dissolved in DMSO (c, 100 mM) and further diluted in a complete Dulbecco's modified Eagle's medium [DMEM; culture medium consisting of 10% fetal bovine serum (FBS)]. The maximum concentration of DMSO even at the highest level of the drugs was less than 0.1% v/v.

Cytotoxicity and Proliferation Assay by MTT Assay. The cytotoxic impacts of **L1**, **1**, and **2** have been explored using the HeLa and HEK293 cells by performing MTT assay.[107] In a typical procedure, the HeLa cells were seeded in a 96-well plate using minimum essential media (MEM; Himedia) containing 10% FBS and 1% penicillin streptomycin and incubated at 37 °C under a humidified CO_2 (5%) environment for 24 h. The cells were treated with **L1**, **1**. and **2** in the concentration range of 20−100 μM for a period of 24 h. Subsequently, media were removed and the cells treated with 0.5 mg mL^{-1} MTT in MEM over a period of an additional 4 h. Later, the MTT-containing media were removed, and 100 μL of DMSO was added to each well. After 15 min of incubation, the plate was read under a Biotek plate reader at 540 nm. The experiment was performed in triplicate. The cytotoxicity against the HEK293 cells was performed by the same protocol using DMEM. The cell viability was calculated using absorbance at 540 nm.

$$\%\text{cell viability} = [\text{mean o.d. of the treated cell/mean o.d. of the control}] \times 100$$

Bioimaging Studies. The cellular uptake for **L1**, **1**, and **2** has been investigated by confocal laser scanning microscopy. HeLa cells were seeded in 27 mm confocal dishes and incubated for 24 h. Further, the cells were treated with **L1**, **1**, and **2** for a period of 4 h and subsequently washed one time with PBS. The intracellular fluorescence was studied using an excitation laser (515 nm) and emission recorded in the range 525−600 nm.

Synthesis. *Synthesis of 6-Methoxy-2-(1H-pyrazol-1-yl)quinoline-3-carbaldehyde (**A**).* **A** was prepared by reacting 2-chloro-6-methoxyquinoline-3-carbaldehyde (2.21 g, 10 mmol) with 1*H*-pyrazole (1.02 g, 15 mmol) in toluene (25 mL) and heating under refluxing conditions with continuous stirring for 48 h. After cooling, the reaction mixture was treated with a saturated $NaHCO_3$ solution and extracted with CH_2Cl_2 (100 mL × 2). The organic layer was separated, dried, and concentrated to dryness under reduced pressure. The crude product thus obtained was purified by column chromatography (SiO_2; ethyl acetate/hexane; 2.02 g, 80%). Anal. Calcd for $C_{14}H_{11}N_3O_2$: C, 66.40; H, 4.38; N, 16.59. Found: C, 66.35; H, 4.34; N, 16.55. ^{1}H NMR ($CDCl_3$): δ 3.93 (s, 3H, OCH_3), 6.56 (s, 1H), 7.24 (d, 2H, J = 7.2 Hz), 7.48 (d, 1H, J = 6.9 Hz), 7.82 (s, 1H), 7.94 (d, 1H, J = 8.7 Hz), 8.65 (s, 2H), 10.67 (s, 1H), 11.25 (s, 1H). IR (KBr pellets, cm^{-1}): 3043, 2872, 1688, 1661, 1614, 1579, 1490, 1455, 1369, 1333, 1165, 1132, 1046, 940, 807, 761, 749.

*Synthesis of 5-[6-Methoxy-2-(1H-pyrazol-1-yl)quinoline]-dipyrromethane (**B**).* Pyrrole (10.0 mL) and catalytic amounts of trifluoroacetic acid (3 drops) were added to a flask containing aldehyde **A** (1.5 g, 5.9 mmol) and the contents of the flask stirred at room temperature for 24 h. After completion of the reaction [monitored by thin-layer chromatography (TLC)], the ensuing solution was concentrated to dryness under reduced pressure. The crude product thus obtained was purified by column chromatography (SiO_2; ethyl acetate/hexane). Yield: 1.63 g, 75%. Anal. Calcd for $C_{22}H_{19}N_5O$: C, 71.53; H, 5.18; N, 18.96. Found: C, 71.46; H, 5.12; N, 18.90. ^{1}H NMR ($CDCl_3$, 300 MHz): δ3.87 (s, 3H, O methyl), 5.89 (s, 2H, pyrrolic H), 6.11 (s, 2H, pyrrolic H), 6.29 (s, 1H, *meso*-H), 6.46 (s, 1H, pyrazole H), 6.70 (s, 2H, pyrrolic H), 6.99 (s, 1H, pyrazole H), 7.33 (d, 1H, J = 9.0 Hz, pyrazole H), 7.79 (s, 1H, aromatic H), 7.88 (d, 1H, J = 9.0 Hz, aromatic H), 8.15 (s, 1H, aromatic H), 8.19 (s, 1H, aromatic H), 9.07 (br, 2H, pyrrolic N−H). ^{13}C NMR ($CDCl_3$, 75 MHz): δ37.6, 55.5, 104.6, 106.4, 106.9, 108.0, 117.3, 123.3, 128.3, 128.9, 130.2, 131.0, 131.1, 132.5, 139.1, 140.7, 141.1, 141.6, 147.1, 158.1. IR (KBr pellets, cm^{-1}): 3412, 3349, 2925, 1595, 1557, 1494, 1448, 1392, 1348, 1281, 1116, 1095, 1041, 940, 778, 768.

*Synthesis of **L1**.* DDQ (0.62 g, 2.7 mmol) dissolved in benzene (50.0 mL) was added dropwise to a solution of **B** (1.0 g, 2.70 mmol) in dichloromethane (15.0 mL) under stirring for 4 h. The reaction mixture was stirred for an additional 2 h. After completion of the reaction, the contents of the flask was concentrated to dryness under reduced pressure. The crude product was dissolved in dichloromethane and filtered to remove any solid impurities. Triethylamine (1.5 mL) and $BF_3{\cdot}Et_2O$ (3.0 mL) were successively added to this solution, and the reaction mixture was stirred for 15 min at room temperature. The progress of the reaction was monitored by TLC. After completion of reaction, it was filtered and the filtrate washed three times with water, extracted with dichloromethane, and concentrated to dryness under reduced pressure. The crude product thus obtained was charged on a flash column (SiO_2; CH_2Cl_2/hexane). The dark-orange-red band was collected and concentrated to dryness to afford the desired product. Yield: 0.34 g, 30%. Anal. Calcd for $C_{22}H_{16}BF_2N_5O$: C, 63.64; H, 3.88; N, 16.87. Found C, 63.58; H, 3.82; N, 16.82. ^{1}H NMR ($CDCl_3$, 500 MHz, a few drops of DMSO-d_6): δ 3.96 (s, 3H, methoxy), 6.31 (d, 1H, J = 1.5 Hz, aromatic H), 6.41 (d, 2H, J = 3.0 Hz, pyrrolic H), 6.69 (d, 2H, J = 3.5 Hz, pyrrolic H), 7.15 (d, 1H, J = 3.0 Hz, aromatic H), 7.44 (s, 1H, J = 2.0 Hz, aromatic H), 7.52 (m, 1H, aromatic H), 7.88 (s, 2H, pyrrolic H), 8.04 (d, 1H, J = 10.0 Hz, aromatic H), 8.24 (s, 1H, aromatic H), 8.36 (d, 1H, J = 3.0 Hz, aromatic H). ^{13}C NMR ($CDCl_3$, 125 MHz, a few drops of DMSO-d_6): δ 55.8, 105.2, 107.9, 118.5, 120.5, 125.0, 126.8, 129.5, 130.2, 135.4, 140.5, 142.1, 143.0, 144.0, 144.6, 158.7. IR (KBr pellets, cm^{-1}): 3106, 2929, 1592, 1557, 1487, 1411, 1387, 1357, 1257, 1140, 1108, 975, 764. ESI-MS. Calcd for $(M + Na)^+$: m/z 438.1314. Found: m/z 438.1351.

*Synthesis of **1**.* The dimeric complex $[(phpy)_2Ir(\mu\text{-}Cl)]_2$ (0.12 g, 0.1 mmol) was added to a suspension of **L1** (0.10 g, 0.24 mmol) in 1:1 CH_2Cl_2/MeOH (50.0 mL) and reaction mixture stirred for 12 h at room temperature. After filtration to remove any solid impurities, a methanolic solution of NH_4PF_6 (0.040 g, 0.25 mmol, 10 mL) was added to it and the resulting mixture stirred for 4 h. The volume of the solution was reduced to half under reduced pressure and precipitated using diethyl ether. The resulting solid was filtered and washed twice with diethyl ether. Yield: 75% (0.16 g). Anal. Calcd for $C_{44}H_{32}BF_8IrN_7OP$: C, 49.82; H, 3.04; N, 9.24. Found: C, 49.75; H, 3.10; N, 9.18. ^{1}H NMR ($CDCl_3$, 500 MHz): δ 3.90 (s, 3H, OCH_3), 6.05 (d, 1H, J = 7.5 Hz, aromatic H), 6.42 (d, 2H, J = 4.5 Hz, aromatic H), 6.45 (d, 1H, J = 3.0 Hz, aromatic H), 6.52 (s, 1H, aromatic H), 6.70 (s, 1H, aromatic H), 6.81 (s, 1H, aromatic H), 6.98−7.07 (m, 6H, aromatic H), 7.24 (d, 2H, J = 3.0 Hz, aromatic H), 7.29 (s, 1H, aromatic H), 7.40 (d, 1H, J = 4.5 Hz, aromatic H), 7.61−7.66 (m, 3H, aromatic H), 7.81 (d, 1H, J = 10.5 Hz, aromatic H), 7.88 (s, 1H, aromatic H), 7.94 (s, 1H, aromatic H), 7.98 (s, 1H, aromatic H), 8.12 (t, 2H, J = 6.5 Hz, aromatic H), 8.22 (d, 1H, J = 6.5 Hz, aromatic H), 8.26 (s, 1H, aromatic H), 8.50 (s, 1H, aromatic H).^{13}C NMR ($CDCl_3$, 125 MHz): δ 56.1 (OCH_3), 106.6, 112.0, 119.8, 122.8, 123.2, 124.1,

DOI: 10.1021/acs.inorgchem.7b01693
Inorg. Chem. XXXX, XXX, XXX−XXX

124.5, 125.3, 127.0, 130.0, 130.5, 130.7, 131.2, 132.0, 134.3, 138.5, 143.1, 144.1, 146.3, 148.5, 150.6 (C_6H_6). ESI-MS. Calcd for $[M - PF_6]^+$: m/z 937.1210. Found: m/z 937.1000.

Synthesis of **2**. **2** was prepared following the above procedure for **1** using $[\{(\eta^5\text{-}C_5Me_5)Ir(\mu\text{-}Cl)Cl\}_2]$ (0.08 g, 0.1 mmol) in place of $[(phpy)_2Ir(\mu\text{-}Cl)]_2$. It was isolated as a red precipitate in good yield. Yield: 73% (0.075 mg). Anal. Calcd for $C_{32}H_{31}BClF_8IrN_5OP$: C, 41.64; H, 3.38; N, 7.58. Found: C, 41.58; H, 3.45; N, 7.52. ^{1}H NMR ($CDCl_3$, 500 MHz): δ 1.59 (s, 15H, methyl), 4.03 (s, 3H, methoxy), 6.54 (d, 1H, J = 4.0 Hz, aromatic H), 6.67 (d, 2H, J = 4.0 Hz, pyrrolic H), 6.71 (m, 2H, pyrrolic H), 7.03 (d, 1H, J = 4.0 Hz, aromatic H), 7.35 (d, 1H, J = 3.0 Hz, aromatic H), 7.65 (m, 1H, aromatic H), 7.94 (d, 1H, J = 2.0 Hz, aromatic H), 8.05 (d, 2H, J = 4.0 Hz, pyrrolic H), 8.39 (d, 1H, J = 9.5 Hz, aromatic H), 8.51 (s, 1H, aromatic H). ^{13}C NMR ($CDCl_3$, 125 MHz): δ56.4, 90.4, 106.8, 112.5, 115.9, 120.3, 121.8, 127.5, 128.8, 130.3, 131.4, 132.1, 134.6, 141.0, 143.9, 146.8, 148.6, 160.4. ESI-MS. Calcd for $[M - PF_6]^+$: m/z 778.1. Found: m/z 778.2.

■ ASSOCIATED CONTENT

Supporting Information

The Supporting Information is available free of charge on the ACS Publications website at DOI: 10.1021/acs.inorgchem.7b01693.

^{1}H and ^{13}C NMR and ESI-MS spectra, UV/vis titration curves, fluorescence spectra, theoretical studies, and tables (PDF)

Accession Codes

CCDC 1553125−1553126 and 1553128 contain the supplementary crystallographic data for this paper. These data can be obtained free of charge via www.ccdc.cam.ac.uk/data_request/cif, or by emailing data_request@ccdc.cam.ac.uk, or by contacting The Cambridge Crystallographic Data Centre, 12 Union Road, Cambridge CB2 1EZ, UK; fax: +44 1223 336033.

■ AUTHOR INFORMATION

Corresponding Author

*E-mail: dspbhu@bhu.ac.in. Tel.: +91 542 6702480.

ORCID

Shaikh M. Mobin: 0000-0003-1940-3822

Daya Shankar Pandey: 0000-0002-6576-4234

Notes

The authors declare no competing financial interest.

■ ACKNOWLEDGMENTS

We thankfully acknowledge the Council of Scientific and Industrial Research, New Delhi, India, for providing financial support through the Scheme 01(2791)/14/EMR-II and also for the award of a Senior Research Fellowship to R.P.P. (Award 09/013(0514)/2013-EMR-I). We are thankful to the Head, Department of Chemistry, Institute of Science, Banaras Hindu University, Varanasi, Uttar Pradesh, India, for extending its laboratory facilities. S.M.M. acknowledges SIC, Indian Institute of Technology Indore, Indore, India, for its confocal facility and SERB, DST, for a research grant. V.S. acknowledge UGC for a research fellowship.

■ REFERENCES

(1) Hartinger, C. G.; Metzler-Nolte, N.; Dyson, P. J. Challenges and Opportunities in the Development of Organometallic Anticancer Drugs. *Organometallics* **2012**, *31*, 5677−5685.

(2) Romero-Canelón, I.; Sadler, P. J. Next-Generation Metal Anticancer Complexes: Multitargeting via Redox Modulation. *Inorg. Chem.* **2013**, *52*, 12276−12291.

(3) Vanrijt, S. H.; Sadler, P. J. Current applications and future potentials for bioinorganic chemistry in the developement of anticancr drugs. *Drug Discovery Today* **2009**, *14*, 1089−1097.

(4) Süss-Fink, G. Areneruthenium complexes as anticancer agents. *Dalton Trans.* **2010**, *39*, 1673−1688.

(5) Gasser, G.; Ott, I.; Metzler-Nolte, N. Organometallic Anticancer Compounds. *J. Med. Chem.* **2011**, *54*, 3−25.

(6) Noffke, A. L.; Habtemariam, A.; Pizarro, A. M.; Sadler, P. J. Designing organometallic compounds for catalysis and therapy. *Chem. Commun.* **2012**, *48*, 5219−5246.

(7) Argyriou, A. A.; Polychronopoulos, P.; Iconomou, G.; Chroni, E.; Kalofonos, H. P. A review on oxaliplatin-induced peripheral nerve damage. *Cancer Treat. Rev.* **2008**, *34*, 368−377.

(8) Johnstone, T. C.; Wilson, J. J.; Lippard, S. J. Monofunctional and Higher-Valent Platinum Anticancer Agents. *Inorg. Chem.* **2013**, *52*, 12234−12249.

(9) Cepeda, V.; Fuertes, M. A.; Castilla, J.; Alonso, C.; Quevedo, C.; Perez, J. M. Biochemical mechanisms of cisplatin cytotoxicity. *Anti-Cancer Agents Med. Chem.* **2007**, *7*, 3−18.

(10) Novohradsky, V.; Liu, Z.; Vojtiskova, M.; Sadler, P. J.; Brabec, V.; Kasparkova, J. Mechanism of cellular accumulation of an iridium(III) pentamethylcyclopentadienyl anticancer complex containing a C,N-chelating ligand. *Metallomics* **2014**, *6*, 682−690.

(11) Liu, Z.; Habtemariam, A.; Pizarro, A. M.; Fletcher, S. A.; Kisova, A.; Vrana, O.; Salassa, L.; Bruijnincx, P. C. A.; Clarkson, G. J.; Brabec, V.; Sadler, P. J. Organometallic Half-sandwich Iridium Anticancer Complexes. *J. Med. Chem.* **2011**, *54*, 3011−3026.

(12) Almodares, Z.; Lucas, S. J.; Crossley, B. D.; Basri, A. M.; Pask, C. M.; Hebden, A. J.; Phillips, R. M.; McGowan, P. C. Rhodium, Iridium, and Ruthenium Half-Sandwich Picolinamide Complexes as Anticancer Agents. *Inorg. Chem.* **2014**, *53*, 727−736.

(13) Peacock, A. F. A.; Sadler, P. J. Medicinal Organometallic Chemistry: Designing Metal Arene Complexes as Anticancer Agents. *Chem. - Asian J.* **2008**, *3*, 1890−1899.

(14) Yellol, G. S.; Donaire, A.; Yellol, J. G.; Vasylyeva, V.; Janiak, C.; Ruiz, J. On the antitumor properties of novel cyclometalated benzimidazole Ru(II), Ir(III) and Rh(III) complexes. *Chem. Commun.* **2013**, *49*, 11533−11535.

(15) Geldmacher, Y.; Oleszak, M.; Sheldrick, W. S. Rhodium(III) and iridium(III) complexes as anticancer agents. *Inorg. Chim. Acta* **2012**, *393*, 84−102.

(16) Chellan, P.; Land, K. M.; Shokar, A.; Au, A.; An, S. H.; Taylor, D.; Smith, P. J.; Riedel, T.; Dyson, P. J.; Chibale, K.; Smith, G. S. Synthesis and evaluation of new polynuclear organometallic Ru(II), Rh(III) and Ir(III) pyridyl ester complexes as in vitro antiparasitic and antitumor agents. *Dalton Trans.* **2014**, *43*, 513−526.

(17) Sava, G.; Zorzet, S.; Perissin, L.; Mestroni, G.; Zassinovich, G.; Bontempi, A. Antineoplastic Activity of Planar Rhodium(I) Complexes in Mice Bearing Lewis Lung Carcinoma and P388 Leukemia. *Inorg. Chim. Acta* **1987**, *137*, 69−71.

(18) Giraldi, T.; Sava, G.; Mestroni, G.; Zassinovich, G.; Stolfa, D. Antitumour Action of Rhodium (I) and Iridium (I) Complexes. *Chem.-Biol. Interact.* **1978**, *22*, 231−238.

(19) He, L.; Li, Yi.; Tan, C. P.; Ye, R. R.; Chen, M. H.; Cao, J. J.; Ji, L. N.; Mao, Z. W. Cyclometalated Iridium(III) Complexes as Lysosome-targeted Photodynamic Anticancer and Real-time Tracking Agents. *Chem. Sci.* **2015**, *6*, 5409−5418.

(20) Kumar, A.; Kumar, A.; Gupta, R. K.; Paitandi, R. P.; Singh, K. B.; Trigun, S. K.; Hundal, M. S.; Pandey, D. S. Cationic Ru(II), Rh(III) and Ir(III) Complexes Containing Cyclic π-perimeter and 2-Aminophenyl Benzimidazole Ligands: Synthesis, Molecular Structure, DNA and Protein Binding, Cytotoxicity and Anticancer Activity. *J. Organomet. Chem.* **2016**, *801*, 68−79.

(21) Farrer, N. J.; Woods, J. A.; Salassa, L.; Zhao, Y.; Robinson, K. S.; Clarkson, G.; Mackay, F. S.; Sadler, P. J. *Angew. Chem., Int. Ed.* **2010**, *49*, 8905−8908.

DOI: 10.1021/acs.inorgchem.7b01693
Inorg. Chem. XXXX, XXX, XXX−XXX

(22) Tripathy, S. K.; De, U.; Dehury, N.; Pal, S.; Kim, H. S.; Patra, S. Dinuclear[[{(p-cym)RuCl}$_2$(μ-phpy)](PF$_6$)$_2$ and heterodinuclear [(ppy)$_2$Ir(μ-phpy)Ru(p-cym)Cl](PF$_6$)$_2$ complexes: synthesis, structure and anticancer activity. *Dalton Trans.* **2014**, *43*, 14546−14549.
(23) Ye, R. R.; Tan, C. P.; Ji, L. N.; Mao, Z. W. Coumarin-appended Phosphorescent Cyclometalated Iridium(III) Complexes as Mitochondria-targeted Theranostic Anticancer Agents. *Dalton Trans.* **2016**, *45*, 13042−13051.
(24) Ye, R. R.; Tan, C. P.; He, L.; Chen, M. H.; Ji, L. N.; Mao, Z. W. Cyclometalated Ir(III) complexes as targeted theranostic anticancer therapeutics: combining HDAC inhibition with photodynamic therapy. *Chem. Commun.* **2014**, *50*, 10945−10948.
(25) Yang, C.; Mehmood, F.; Lam, T. L.; Chan, S. L. F.; Wu, Y.; Yeung, C. S.; Guan, X.; Li, K.; Chung, C. Y. S.; Zhou, C. Y.; Zou, T.; Che, C. M. Stable luminescent iridium(III) complexes with bis(N-heterocyclic carbene) ligands: photo-stability, excited state properties, visible-light-driven radical cyclization and CO_2 reduction, and cellular imaging. *Chem. Sci.* **2016**, *7*, 3123−3136.
(26) Zimbron, J. M.; Passador, K.; Gatin-Fraudet, B.; Bachelet, C. M.; Plażuk, D.; Chamoreau, L. M.; Botuha, C.; Thorimbert, S.; Salmain, M. Synthesis, Photophysical Properties, and Living Cell Imaging of Theranostic Half-Sandwich Iridium−4,4-Difluoro-4-bora-3a,4a-diaza-s-indacene (BODIPY) Dyads. *Organometallics* **2017**, *36*, 3435.
(27) Chi, Y.; Chou, P. T. Transition-metal phosphors with cyclometalating ligands: fundamentals and applications. *Chem. Soc. Rev.* **2010**, *39*, 638−655.
(28) Lowry, M. S.; Bernhard, S. Synthetically Tailored Excited States: Phosphorescent, Cyclometalated Iridium(III) Complexes and Their Applications. *Chem. - Eur. J.* **2006**, *12*, 7970−7977.
(29) Majumdar, P.; Yuan, X.; Li, S.; Le Guennic, B.; Ma, J.; Zhang, C.; Jacquemin, D.; Zhao, J. Cyclometalated Ir(III) complexes with styrylBODIPY ligands showing near IR absorption/emission: preparation, study of photophysical properties and application as photodynamic/luminescence imaging materials. *J. Mater. Chem. B* **2014**, *2*, 2838−2854.
(30) Lo, K. K.; Zhang, K. Y.; Leung, S. K.; Tang, M. C. Exploitation of the Dual-Emissive Properties of Cyclometalated Iridium(III)-Polypyridine Complexes in the Development of Luminescent Biological Probes. *Angew. Chem., Int. Ed.* **2008**, *47*, 2213−2216.
(31) Chen, Y.; Qiao, L.; Ji, L.; Chao, H. Phosphorescent iridium(III) complexes as multicolor probes for specific mitochondrial imaging and tracking. *Biomaterials* **2014**, *35*, 2−13.
(32) Lo, K. K. W.; Zhang, K. Y. Iridium(III) complexes as therapeutic and bioimaging reagents for cellular applications. *RSC Adv.* **2012**, *2*, 12069−12083.
(33) Liu, J.; Jin, C.; Yuan, B.; Liu, X.; Chen, Y.; Ji, L.; Chao, H. Selectively lighting up two- photon photodynamic activity in mitochondria with AIE-active iridium(III) complexes. *Chem. Commun.* **2017**, *53*, 2052−2055.
(34) Yu, M.; Zhao, Q.; Shi, L.; Li, F.; Zhou, Z.; Yang, H.; Yi, T.; Huang, C. Cationic iridium(III) complexes for phosphorescence staining in the cytoplasm of living cells. *Chem. Commun.* **2008**, 2115−2117.
(35) Mukhopadhyay, S.; Gupta, R. K.; Paitandi, R. P.; Rana, N. K.; Sharma, G.; Koch, B.; Rana, L. K.; Hundal, M. S.; Pandey, D. S. Synthesis, Structure, DNA/Protein Binding, and Anticancer Activity of Some Half-Sandwich Cyclometalated Rh(III) and Ir(III) Complexes. *Organometallics* **2015**, *34*, 4491−4506.
(36) Wang, C.; Liu, J.; Tian, Z.; Tian, M.; Tian, L.; Zhao, W.; Liu, Z. Half-sandwich iridium N-heterocyclic carbine anticancer complexes. *Dalton Trans.* **2017**, *46*, 6870−6883.
(37) Tabrizi, L.; Chiniforoshan, H. New cyclometalated Ir(III) complexes with NCN pincer and meso-phenylcyanamide BODIPY ligands as efficient photodynamic therapy agents. *RSC Adv.* **2017**, *7*, 34160−34169.
(38) Loughrey, B. T.; Healy, P. C.; Parsons, P. G.; Williams, M. L. Selective Cytotoxic Ru(II) Arene Cp* Complex Salts [R-PhRuCp*]$^+$X$^-$ for X = BF_4^-, PF_6^-, and BPh_4^-. *Inorg. Chem.* **2008**, *47*, 8589−8591.
(39) Liu, Z.; Sadler, P. J. Organoiridium Complexes: Anticancer Agents and Catalysts. *Acc. Chem. Res.* **2014**, *47*, 1174−1185.
(40) Ruiz, J.; Vicente, C.; de Haro, C.; Bautista, D. Novel Bis-C,N-cyclometalated Iridium(III) Thiosemicarbazide Antitumor Complexes: Interactions with Human Serum Albumin and DNA, and Inhibition of Cathepsin B. *Inorg. Chem.* **2013**, *52*, 974−982.
(41) Gupta, G.; Das, A.; Ghate, N. B.; Kim, T.; Ryu, J. Y.; Lee, J.; Mandal, N.; Lee, C. Y. Novel BODIPY-based Ru(II) and Ir(III) metallarectangles: cellular localization of compounds and their antiproliferative activities. *Chem. Commun.* **2016**, *52*, 4274−4277.
(42) Hisamatsu, Y.; Shibuya, A.; Suzuki, N.; Suzuki, T.; Abe, R.; Aoki, S. Design and Synthesis of Amphiphilic and Luminescent Tris-Cyclometalated Iridium(III) Complexes Containing Cationic Peptides as Inducers and Detectors of Cell Death via a Calcium-Dependent Pathway. *Bioconjugate Chem.* **2015**, *26*, 857−879.
(43) Liu, Z.; Romero-Canelón, R. I.; Qamar, B.; Hearn, J. M.; Habtemariam, A.; Barry, N. P. E.; Pizarro, A. M.; Clarkson, G. J.; Sadler, P. J. The Potent Oxidant Anticancer Activity of Organoiridium Catalysts. *Angew. Chem.* **2014**, *126*, 4022−4027.
(44) Li, S. P. Y.; Lau, C. T. S.; Louie, M. W.; Lam, Y. W.; Cheng, S. H.; Lo, K. K. W. Mitochondria-targeting cyclometalated iridium(III)-PEG complexes with tunable photodynamic activity. *Biomaterials* **2013**, *34*, 7519−7532.
(45) Liu, Z.; Romero-Canelón, I.; Habtemariam, A.; Clarkson, G. J.; Sadler, P. J. Potent Half-Sandwich Iridium(III) Anticancer Complexes Containing C^N-Chelated and Pyridine Ligands. *Organometallics* **2014**, *33*, 5324−5333.
(46) Lau, J. S.Y.; Lee, P. K.; Tsang, K. H. K.; Ng, C. H. C.; Lam, Y. W.; Cheng, S. H.; Lo, K. K. W. Luminescent Cyclometalated Iridium(III) Polypyridine Indole Complexes: Synthesis, Photophysics, Electrochemistry, Protein-Binding Properties, Cytotoxicity, and Cellular Uptake. *Inorg. Chem.* **2009**, *48*, 708−718.
(47) Lucas, S. J.; Lord, R. M.; Wilson, R. L.; Phillips, R. M.; Sridharan, V.; McGowan, P. C. Synthesis of iridium and ruthenium complexes with (N,N), (N,O) and (O,O) coordinating bidentate ligands aspotential anti-cancer agents. *Dalton Trans.* **2012**, *41*, 13800.
(48) Liu, Z.; Habtemariam, A.; Pizarro, A. M.; Clarkson, G. J.; Sadler, P. J. Organometallic Iridium(III) Cyclopentadienyl Anticancer Complexes Containing C,N-Chelating Ligands. *Organometallics* **2011**, *30*, 4702−4710.
(49) Liu, Z.; Salassa, L.; Habtemariam, A.; Pizarro, A. M.; Clarkson, G. J.; Sadler, P. J. Contrasting Reactivity and Cancer Cell Cytotoxicity of Isoelectronic Organometallic Iridium(III) Complexes. *Inorg. Chem.* **2011**, *50*, 5777−5783.
(50) Millett, A. J.; Habtemariam, A.; Romero-Canelón, I.; Clarkson, G. J.; Sadler, P. J. Contrasting Anticancer Activity of Half-Sandwich Iridium(III) Complexes Bearing Functionally Diverse 2-Phenylpyridine Ligands. *Organometallics* **2015**, *34*, 2683−2694.
(51) Ali Nazif, M.; Bangert, J. A.; Ott, I.; Gust, R.; Stoll, R.; Sheldrick, W. S. Dinuclear Organoiridium(III) Mono- and Bis-intercalators with Rigid Bridging Ligands: Synthesis, Cytotoxicity and DNA Binding. *J. Inorg. Biochem.* **2009**, *103*, 1405−1414.
(52) Schäfer, S.; Sheldrick, W. S. Coligand tuning of the DNA binding properties of half-sandwich organometallic intercalators: Influence of polypyridyl (pp) and monodentate ligands (L = Cl, $(NH_2)_2$CS, $(NMe_2)_2$CS) on the intercalation of (g5-entamethylcyclopentadienyl)-iridium(III)- dipyridoquinoxaline and dipyridophenazine complexes. *J. Organomet. Chem.* **2007**, *692*, 1300−1309.
(53) Gupta, R. K.; Pandey, R.; Sharma, G.; Prasad, R.; Koch, B.; Srikrishna, S.; Li, P. Z.; Xu, Q.; Pandey, D. S. DNA Binding and Anti-Cancer Activity of Redox-Active Heteroleptic Piano-Stool Ru(II), Rh(III), and Ir(III) Complexes Containing 4-(2 Methoxypyridyl) phenyldipyrromethene. *Inorg. Chem.* **2013**, *52*, 3687−3698.
(54) Zhao, C.; Zhang, Y.; Wang, X.; Cao, J. Development of BODIPY-based fluorescent DNA intercalating probes. *J. Photochem. Photobiol., A* **2013**, *264*, 41−47.
(55) Kamkaew, A.; Lim, S. H.; Lee, H. B.; Kiew, L. V.; Chung, L. Y.; Burgess, K. BODIPY dyes in photodynamic therapy. *Chem. Soc. Rev.* **2013**, *42*, 77−88.

DOI: 10.1021/acs.inorgchem.7b01693
Inorg. Chem. XXXX, XXX, XXX−XXX

(56) Gupta, G.; Das, A.; Park, K. C.; Tron, A.; Kim, H.; Mun, J.; Mandal, N.; Chi, K. W.; Lee, C. Y. Self-Assembled Novel BODIPY-Based Palladium Supramolecules and Their Cellular Localization. *Inorg. Chem.* **2017**, *56*, 4615−4621.
(57) Paitandi, R. P.; Gupta, R. K.; Singh, R. S.; Sharma, G.; Koch, B.; Pandey, D. S. Interaction of ferrocene appended Ru(II), Rh(III) and Ir(III) dipyrrinato complexes with DNA/protein, molecular docking and antitumor activity. *Eur. J. Med. Chem.* **2014**, *84*, 17−29.
(58) Gupta, R. K.; Sharma, G.; Pandey, R.; Kumar, A.; Koch, B.; Li, P. Z.; Xu, Q.; Pandey, D. S. DNA/Protein Binding, Molecular Docking, and in Vitro Anticancer Activity of Some Thioether-Dipyrrinato Complexes. *Inorg. Chem.* **2013**, *52*, 13984−13996.
(59) Srivastava, A.; Singh, R. M. Vilsmeier−Haack reagent:A facile synthesis of 2-chloro3-formylquinolines from N-arylacetamides and transformation into different functionalities. *Indian J. Chem., Sect. B* **2006**, *37*, 1868−1875.
(60) Loudet, A.; Burgess, K. BODIPY Dyes and Their Derivatives: Syntheses and Spectroscopic Properties. *Chem. Rev.* **2007**, *107*, 4891−4932.
(61) Singh, R. S.; Gupta, R. K.; Paitandi, R. P.; Dubey, M.; Sharma, G.; Koch, B.; Pandey, D. S. Morphological tuning via structural modulations in AIE luminogens with the minimum number of possible variables and their use in live cell imaging. *Chem. Commun.* **2015**, *51*, 9125−9128.
(62) Jacques, A.; Kirsch-De Mesmaeker, A.; Elias, B. Selective DNA Purine Base Photooxidation by Bis-terdentate Iridium(III) Polypyridyl and Cyclometalated Complexes. *Inorg. Chem.* **2014**, *53*, 1507−1512.
(63) Nakagawa, A.; Hisamatsu, Y.; Moromizato, S.; Kohno, M.; Aoki, S. Selective DNA Purine Base Photo-oxidation by Bis-terdentate Iridium(III) Polypyridyl and Cyclometalated Complexes. *Inorg. Chem.* **2014**, *53*, 409−422.
(64) Hanson, K.; Tamayo, A.; Diev, V. V.; Whited, M. T.; Djurovich, P. I.; Thompson, M. E. Efficient Dipyrrin-Centered Phosphorescence at Room Temperature from Bis-Cyclometalated Iridium(III) Dipyrrinato Complexes. *Inorg. Chem.* **2010**, *49*, 6077−6084.
(65) Mukhopadhyay, S.; Singh, R. S.; Biswas, A.; Maiti, B.; Pandey, D. S. Molecular and Nanoaggregation in Cyclometalated Iridium(III) Complexes through Structural Modification. *Eur. J. Inorg. Chem.* **2016**, *2016*, 4199−4206.
(66) Madhu, S.; Kumar, S.; Chatterjee, T.; Ravikanth, M. Synthesis, X-ray structure, spectral and electrochemical properties of a b-meso covalently linked BODIPY−Ru(II) dipyrrin complex. *New J. Chem.* **2014**, *38*, 5551−5558.
(67) Rachford, A. A.; Ziessel, R.; Bura, T.; Retailleau, P.; Castellano, F. N. Boron Dipyrromethene (Bodipy) Phosphorescence Revealed in $[Ir(ppy)_2(bpy\text{-}C{\equiv}C\text{-}Bodipy)]^+$. *Inorg. Chem.* **2010**, *49*, 3730−3736.
(68) Wang, T.; Hou, Y.; Chen, Y.; Li, K.; Cheng, X.; Zhou, Q.; Wang, X. Two novel BODIPY−Ru(II) arene dyads enabling effective photoinactivation against cancer cells Dalton. *Trans.* **2015**, *44*, 12726−12734.
(69) Ganeshpandian, M.; Loganathan, R.; Suresh, E.; Riyasdeen, A.; Akbarsha, M. A.; Palaniandavar, M. New ruthenium(II) arene complexes of anthracenyl-appended diazacycloalkanes: effect of ligand intercalation and hydrophobicity on DNA and protein binding and cleavage and cytotoxicity. *Dalton Trans.* **2014**, *43*, 1203−1219.
(70) Alagesan, M.; Sathyadevi, P.; Krishnamoorthy, P.; Bhuvanesh, N. S. P.; Dharmaraj, N. DMSO containing ruthenium(II) hydrazone complexes: in vitro evaluation of biomolecular interaction and anticancer activity. *Dalton Trans.* **2014**, *43*, 15829−15840.
(71) Kilpin, K. J.; Clavel, C. M.; Edafe, F.; Dyson, P. J. Naphthalimide-Tagged Ruthenium−Arene Anticancer Complexes: Combining Coordination with Intercalation. *Organometallics* **2012**, *31*, 7031−7039.
(72) Hu, K.; Li, F.; Zhang, Z.; Liang, F. Synthesis of two potential anticancer copper(II) complex drugs: their crystal structure, human serum albumin/DNA binding and anticancer mechanism. *New J. Chem.* **2017**, *41*, 2062−2072.
(73) Rizvi, M. A.; Zaki, M.; Afzal, M.; Mane, M.; Kumar, M.; Shah, B. A.; Srivastav, S.; Srikrishna, S.; Peerzada, G. M.; Tabassum, S. Nuclear blebbing of biologically active organoselenium compound towards human cervical cancer cell (HeLa): In vitro DNA/HSA binding, cleavage and cell imaging studies. *Eur. J. Med. Chem.* **2015**, *90*, 876−888.
(74) Keck, M. V.; Lippard, S. J. Unwinding of supercoiled DNA by platinum-ethidium and related complexes. *J. Am. Chem. Soc.* **1992**, *114*, 3386−3390.
(75) Liu, Z. C.; Wang, B. D.; Yang, Z. Y.; Li, Y.; Qin, D. D.; Li, T. R. Synthesis, crystal structure, DNA interaction and antioxidant activities of two novel water-soluble Cu^{2+} complexes derivated from 2-oxo-quinoline-3-carbaldehyde Schiff-bases. *Eur. J. Med. Chem.* **2009**, *44*, 4477−4484.
(76) Paitandi, R. P.; Singh, R. S.; Mukhopadhyay, S.; Sharma, G.; Koch, B.; Vishnoi, P.; Pandey, D. S. Synthesis, characterization, DNA binding and cytotoxicity of fluoro-dipyrrin based arene ruthenium(II) complexes. *Inorg. Chim. Acta* **2017**, *454*, 117−127.
(77) Senthil Raja, D.; Bhuvanesh, N. S. P.; Natarajan, K. Biological evaluation of a novel water soluble sulphur bridged binuclear copper(II) thiosemicarbazone complex. *Eur. J. Med. Chem.* **2011**, *46*, 4584−4594.
(78) Dang, C. V.; Ebert, R. F.; Bell, W. R. binding site between gamma-subunit positions 311 and 336 by terbium fluorescence. *J. Biol. Chem.* **1985**, *260*, 9713−9719.
(79) Ramachandran, E.; Thomas, S. P.; Poornima, P.; Kalaivani, P.; Prabhakaran, R.; Padma, V. V.; Natarajan, K. Evaluation of DNA binding, antioxidant and cytotoxic activity of mononuclear Co(III) complexes of 2-oxo-1,2-dihydrobenzo[h]quinoline-3-carbaldehyde thiosemicarbazones. *Eur. J. Med. Chem.* **2012**, *50*, 405−415.
(80) Bhattacharyya, M.; Chaudhuri, U.; Poddar, R. K. Evidence for cooperative binding of chlorpromazine with hemoglobin: Equilibrium dialysis, fluorescence quenching and oxygen release study. *Biochem. Biophys. Res. Commun.* **1990**, *167*, 1146−1153.
(81) Wang, C. X.; Yan, F. F.; Zhang, Y. X.; Ye, L. Spectroscopic investigation of the interaction between rifabutin and bovine serum albumin. *J. Photochem. Photobiol., A* **2007**, *192*, 23−28.
(82) Raja, D. S.; Bhuvanesh, N. S. P.; Natarajan, K. A novel water soluble ligand bridged cobalt(II) coordination polymer of 2-oxo-1,2-dihydroquinoline-3-carbaldehyde (isonicotinic) hydrazone: evaluation of the DNA binding, protein interaction, radical scavenging and anticancer activity. *Dalton Trans.* **2012**, *41*, 4365−4375.
(83) Miller, J. N. Recent advances in molecular luminescence analysis. *Proc. Anal. Div. Chem. Soc.* **1979**, *16*, 203−208.
(84) Burstein, E. A.; Vedenkina, N. S.; Ivkova, M. N. Fluorescence and the location of tryptophan residues in protein molecules. *Photochem. Photobiol.* **1973**, *18*, 263−279.
(85) Bernhardt, P. V.; Sharpe, P. C.; Islam, M.; Lovejoy, D. B.; Kalinowski, D. S.; Richardson, D. R. Iron Chelators of the Dipyridylketone Thiosemicarbazone Class: Precomplexation and Transmetalation Effects on Anticancer Activity. *J. Med. Chem.* **2009**, *52*, 407−415.
(86) Tong, J. Q.; Tian, F. F.; Li, Q.; Li, L. L.; Xiang, C.; Liu, Y.; Dai, J.; Jiang, F. L. Probing the adverse temperature dependence in the static fluorescence quenching of BSA induced by a novel anticancer hydrazon. *Photochem. Photobiol. Sci.* **2012**, *11*, 1868−1879.
(87) Holm, A. I. S.; Nielsen, L. M.; Hoffmann, S. V.; Nielsen, S. B. Vacuum-ultraviolet circular dichroism spectroscopy of DNA: A valuable tool to elucidate topology and electronic coupling in DNA. *Phys. Chem. Chem. Phys.* **2010**, *12*, 9581−9596.
(88) Chang, Y. M.; Chen, C. K. M.; Hou, M. H. Conformational changes in DNA upon ligand binding monitored by circular dichroism. *Int. J. Mol. Sci.* **2012**, *13*, 3394−3413.
(89) Cutts, S. M.; Masta, A.; Panousis, C.; Parsons, P. G.; Sturm, R. A.; Phillips, D. R. A Gel Mobility Shift Assay for Probing the Effect of Drug−DNA Adducts on DNA-Binding Proteins. *Drug-DNA Interact, Protocols* **1997**, *90*, 95−106.
(90) Suh, D.; Chaires, J. B. Criteria for the mode of binding of DNA binding agents. *Bioorg. Med. Chem.* **1995**, *3*, 723−728.
(91) Rajendiran, V.; Murali, M.; Suresh, E.; Sinha, S.; Somasundaram, K.; Palaniandavar, M. Mixed ligand ruthenium(II) complexes of

DOI: 10.1021/acs.inorgchem.7b01693
Inorg. Chem. XXXX, XXX, XXX−XXX

bis(pyrid-2-yl)-/bis(benzimidazol- 2-yl)-dithioether and diimines: Study of non-covalent DNA binding and cytotoxicity. *Dalton Trans.* **2008**, 148−163.
(92) Kelly, J. M.; Tossi, A. B.; McConnell, D. J.; OhUigin, O. A study of the interactions of some polypyridylruthenium (II) complexes with DNA using fluorescence spectroscopy, topoisomerisation and thermal denaturation. *Nucleic Acids Res.* **1985**, *13*, 6017−6034.
(93) Inclán, M.; Albelda, M. T.; Frías, J. C.; Blasco, S.; Verdejo, B.; Serena, C.; Salat-Canela, C.; Díaz, M. L.; García-España, A.; García-España, E. Modulation of DNA Binding by Reversible Metal-Controlled Molecular Reorganizations of Scorpiand-like Ligands. *J. Am. Chem. Soc.* **2012**, *134*, 9644−9656.
(94) Martins, S.; Sarmento, B.; Ferreira, D. C.; Souto, E. B. Lipid-based Colloidal Carriers for Peptide and Protein Delivery-liposomes Versus Lipid Nanoparticles. *Int. J. Nanomed.* **2007**, *2*, 595−607.
(95) Oldfield, S. P.; Hall, M. D.; Platts, J. A. Calculation of Lipophilicity of a Large, Diverse Dataset of Anticancer Platinum Complexes and the Relation to Cellular Uptake. *J. Med. Chem.* **2007**, *50*, 5227−5237.
(96) Vock, C. A.; Renfrew, A. K.; Scopelliti, R.; Juillerat-Jeanneret, L.; Dyson, P. J. Influence of the Diketonato Ligand on the Cytotoxicities of $[Ru(\eta^6\text{-p-cymene})(R_2acac)(PTA)]^+$ Complexes (PTA = 1,3,5-triaza-7-phosphaadamantane). *Eur. J. Inorg. Chem.* **2008**, *2008*, 1661−1671.
(97) Mustard, D.; Ritchie, D. W. Docking essential dynamics eigenstructures. *Proteins: Struct., Funct., Genet.* **2005**, *60*, 269−274.
(98) Husain, M. A.; Sarwar, T.; Rehman, S. U.; Ishqi, H. M.; Tabish, M. Ibuprofen causes photocleavage through ROS generation and intercalates with DNA: a combined biophysical and molecular docking approach. *Phys. Chem. Chem. Phys.* **2015**, *17*, 13837−13850.
(99) Tabassum, S.; Zaki, M.; Afzal, M.; Arjmand, F. New Modulated Design and Synthesis of Quercetin-Cu(II)/Zn(II)-Sn_2(IV) Scaffold as Anticancer Agents: In vitro DNA Binding Profile, DNA Cleavage Pathway and Topo-I Activity. *Dalton Trans.* **2013**, *42*, 10029−10041.
(100) Filosa, R.; Peduto, A.; Micco, S. D.; Caprariis, P. D.; Festa, M.; Petrella, A.; Capranico, G.; Bifulco, G. Molecular Modelling Studies, Synthesis and Biological Activity of a Series of Novel Bisnaphthalimides and their Development as New DNA Topoisomerase II Inhibitors. *Bioorg. Med. Chem.* **2009**, *17*, 13−24.
(101) Tabassum, S.; Al-Asbahy, W. M.; Afzal, M.; Arjmand, F.; Hasan Khan, R. Interaction and Photo-induced Cleavage Studies of a Copper Based Chemotherapeutic Drug with Human Serum Albumin: Spectroscopic and Molecular Docking Study. *Mol. BioSyst.* **2012**, *8*, 2424−2433.
(102) Frisch, M. J.; Trucks, G. W.; Schlegel, H. B.; Scuseria, G. E.; Robb, M. A.; Cheeseman, J. R.; Scalmani, G.; Barone, V.; Mennucci, B.; Petersson, G. A.; Nakatsuji, H.; Caricato, M.; Li, X.; Hratchian, H. P.; Izmaylov, A. F.; Bloino, J.; Zheng, G.; Sonnenberg, J. L.; Hada, M.; Ehara, M.; Toyota, K.; Fukuda, R.; Hasegawa, J.; Ishida, M.; Nakajima, T.; Honda, Y.; Kitao, O.; Nakai, H.; Vreven, T.; Montgomery, J. A., Jr.; Peralta, J. E.; Ogliaro, F.; Bearpark, M.; Heyd, J. J.; Brothers, E.; Kudin, K. N.; Staroverov, V. N.; Kobayashi, R.; Normand, J.; Raghavachari, K.; Rendell, A.; Burant, J. C.; Iyengar, S. S.; Tomasi, J.; Cossi, M.; Rega, N.; Millam, N. J.; Klene, M.; Knox, J. E.; Cross, J. B.; Bakken, V.; Adamo, C.; Jaramillo, J.; Gomperts, R.; Stratmann, R. E.; Yazyev, O.; Austin, A. J.; Cammi, R.; Pomelli, C.; Ochterski, J. W.; Martin, R. L.; Morokuma, K.; Zakrzewski, V. G.; Voth, G. A.; Salvador, P.; Dannenberg, J. J.; Dapprich, S.; Daniels, A. D.; Farkas, Ö.; Foresman, J. B.; Ortiz, J. V.; Cioslowski, J.; Fox, D. J. *Gaussian 09*, revision A.1; Gaussian, Inc.: Wallingford, CT, 2009.
(103) Krishnan, R.; Binkley, J. S.; Seeger, R.; Pople, J. A. Self-consistent molecular orbital methods. XX. A basis set for correlated wave functions. *J. Chem. Phys.* **1980**, *72*, 650.
(104) Wadt, W. R.; Hay, P. Ab initio effective core potentials for molecular calculations. Potentials for main group elements Na to Bi. *J. Chem. Phys.* **1985**, *82*, 284.
(105) Becke, A. D. Density-functional thermochemistry. III. The role of exact exchange. *J. Chem. Phys.* **1993**, *98*, 5648.
(106) Lee, C. T.; Yang, W. T.; Parr, R. G. Development of the Colle-Salvetti correlation-energy formula into a functional of the electron density. *Phys. Rev. B: Condens. Matter Mater. Phys.* **1988**, *37*, 785−789.
(107) Berridge, M. V.; Herst, P. M.; Tan, A. S. Tetrazolium dyes as tools in cell biology: new insights into their cellular reduction. *Biotechnol. Annu. Rev.* **2005**, *11*, 127−152.
(108) Mukhopadhyay, S.; Singh, R. S.; Paitandi, R. P.; Sharma, G.; Koch, B.; Pandey, D. S. Influence of Substituents on DNA/ Protein Binding and Anticancer Activity of Cyclometalated Ir(III) Complexes. *Dalton Trans.* **2017**, *46*, 8572−8585.
(109) Bezabeh, T.; Mowat, M. R. A.; Jarolim, L.; Greenberg, A. H.; Smith, I. C. P. Detection of drug-induced apoptosis and necrosis inhuman cervical carcinoma cells using ^{1}H NMR spectroscopy. *Cell Death Differ.* **2001**, *8*, 219−224.
(110) Perrin, D. D.; Armango, W. L. F.; Perrin, D. R. *Purification of laboratory Chemicals*; Pergamon: Oxford, U.K., 1986.
(111) Sheldrick, G. M. *SHELXL-97, Program for X-ray Crystal Structure Refinement*; Gottingen University: Gottingen, Germany, 1997.
(112) Sheldrick, G. M.; *SHELXS-97, Program for X-ray Crystal Structure Solution*; Gottingen University: Gottingen, Germany, 1997.
(113) Spek, A. L. *PLATON, A Multipurpose Crystallographic Tools*; Utrecht University: Utrecht, The Netherlands, 2000.
(114) Spek, A. L. *Acta Crystallogr., Sect. A* **1990**, *46*, C31.

DOI: 10.1021/acs.inorgchem.7b01693
Inorg. Chem. XXXX, XXX, XXX−XXX